Early-Middle Paleozoic Andes-type Continental Margin in the Chifeng Area, Inner Mongolia: Framework, Geochronology and Geochemistry and Implications for Tectonic Evolution of the Central Asian Orogenic Belt

YAN Linjie[1], XU Bei[1, 2, *], ZHANG Jiaming[1] and WANG Yanyang[1]

[1] *Key Laboratory of Orogenic Belts and Evolution, Peking University, Beijing 100871, China*
[2] *Key Laboratory of Regional Geology and Mineralization, Hebei GEO University, Shijiazhuang 050031, China*

Abstract: Three tectonic units have been recognized in the Chifeng area, Inner Mongolia, from north to south, including the Qiganmiao accretionary prism, Jiefangyingzi arc belt and Sidaozhangpeng molasse basin, which formed an Andean-type active continent margin during the early to middle Paleozoic. The Qiganmiao accretionary prism is characterized by a mélange that consists of gabbro, two-mica quartz schist and basic volcanic rock blocks and heterogeneously deformed marble matrix. Two zircon U-Pb ages of 446.0±6.3 Ma and 1104±27 Ma have been acquired and been interpreted as the metamorphic and forming ages for the gabbro and two-mica quartz schist, respectively. The prism formed during the early to middle Paleozoic southward subduction of the Paleo Asian Ocean (PAO) and represents a suture between the North China craton (NCC) and Central Asian Orogenic Belt (CAOB). The Jiefangyingzi arc belt consists of pluton complex and volcanic rocks of the Xibiehe and Badangshan Formations, and Geochronology analysis indicates that the development of it can be divided into two stages. The first stage is represented by the Xibiehe Formation volcanic rocks, which belong to the subalkaline series, enriched LREE and LILE and depleted HFSE, with negative Eu anomalies, and plot in the volcanic arc field in discrimination diagrams. These characters indicate that the Xibiehe Formation results from to the continental arc magmatic activity related to the subduction of the PAO during 400–420 Ma. Magmatism of the second stage in 380–390 Ma consists of the Badangshan Formation volcanic rocks. Geochemistry analysis reveals that rhyolite, basaltic andesite and basalt of the Badangshan Formation were developed in continental margin arc setting. Moreover, the basaltic andesite and basalt display positive Sr anomalies, and the basalt have very low Nb/La values, suggesting that fluid is involved in magma evolution and the basalts were contaminated by continental crust. The sequence of Sidaozhangpeng molasse basin is characterized by proximity, coarseness and large thickness, similar to the proximity molasses basin. According to our field investigation, geochronological and geochemical data, combined with previous research in this area, a tectonic evolutionary model for Andes-type active continental margin of the CAOB has been proposed, including a development of the subduction-free PAO before 446 Ma, a subduction of the PAO and arc-related magmatism during 446–380 Ma, and formation of a molasse basin during 380–360 Ma.

Key words: Chifeng area, andes-type continental margin, early-middle paleozoic, tectonic evolution, Central Asian Orogenic Belt

Citation: Yan et al., 2020. Early-Middle Paleozoic Andes-type Continental Margin in the Chifeng Area, Inner Mongolia: Framework, Geochronology and Geochemistry and Implications for Tectonic Evolution of the Central Asian Orogenic Belt. Acta Geologica Sinica (English Edition), 94(1): 57–74. DOI: 10.1111/1755-6724.14400

1 Introduction

The Central Asian Orogenic Belt (CAOB) is located between the Siberian craton in the north and the North China and Tarim cratons in the south, which is characterized by a series of island arcs, forearc or backarc basins, ophiolitic belts and microcontinents from the Neoproterozoic to Mesozoic (Hsü et al., 1991; Mossakovsky et al., 1993; Sengör et al., 1993; Sengör and Natal'in, 1996; Badarch et al., 2002; Khain et al., 2002; 2003; Xiao et al., 2003; 2004; 2009; Li, 2006; Kröner et al., 2007; 2010a; 2010b; Demoux et al., 2009) and its massive generation of juvenile crust in the Phanerozoic (Hong et al., 1996; 2003; Han et al., 1997; 2011; Jahn et al., 2000a; 2000b; 2009). The northeast China and Inner Mongolia belong to southeastern part of the CAOB, where a convergent orogenic belt has been identified, including the Northern Orogenic Belt (NOB), Southern Orogenic Belt (SOB) and the Songliao Hunshandake Block between them (SHB, Xu and Chen1993; 1997; Xu et al., 2013; Jian et al., 2008).

The NOB extends ca. 550 km from Xilinhot in the east to Airgin Sum areas in the west and five units have been recognized from north to south: including back-arc basin, arc-pluton complex, accretionary prism, molasses basin, and fold belt (Fig. 1; Xu and Chen, 1997; Xu et al., 2013;

* Corresponding author. E-mail: bxu@pku.edu.cn

Li et al., 2014; Zhang et al., 2018; Chen et al., 2000; 2009). The back arc basin occurs only in Baiyanbaolidao area（He et al., 2018）. The arc-pluton complex extends discontinuously in Airgin Sum, Baiyanbaolidao, and Xilinhot areas from west to east. The accretionary prism can be discontinuously traced in Airgin Sum, ErdaoJing, Naomuhunni and Honger areas, from west to east. The molasse basin occurs near the accretionary prism or arc-pluton complex to the south of Abag and Baiyanbaolidao. The fold belt crops out in the southern area (Fig. 1).

The SOB extends from Ondor Sum, via Bater, to Tugurige, with a length of ca. 600 km from west to east. It has been defined based on detail study of ophiolite, arc pluton, accretionary prism and fold deformation in Ondor Sum and Bater areas (Shao, 1986; Hu et al., 1990; Tang and Zhang, 1991; Xiao et al., 2003; Jian et al., 2008; Liao et al., 2015). Four units have been recognized, from north to south: fold belt, accretionary prism, arc magmatic belt and back-arc basin (Xu et al., 2013). Composed of the early Paleozoic Ondor Sum Group, the fold belt is found in both Tugurige, Hongqi and Ondor Sum areas (Shi et al., 2013). The accretionary prism is characterized by a south-dipping subduction-accretion complex that extends westwards from Ondor Sum (Hu, et al., 1990; Tang, et al., 1992; Xiao, et al., 2003) and Bater to Tugurige areas (Xu et al., 2013; Liao et al., 2015). To the south of the accrtionary prism an arc magmatic belt including volcanic rocks and plutons can be traced from Boin Sum, Bater (Jian, et al., 2008) to Tugurige areas. To the south of the arc magmatic belt, the back-arc basin belt occurs in Tugurige, Bater and Boin Sum areas, with flysch in lower part and molasse in upper part (Zhang and Tang, 1989; Hu et al., 1990; Tang, et al., 1992;

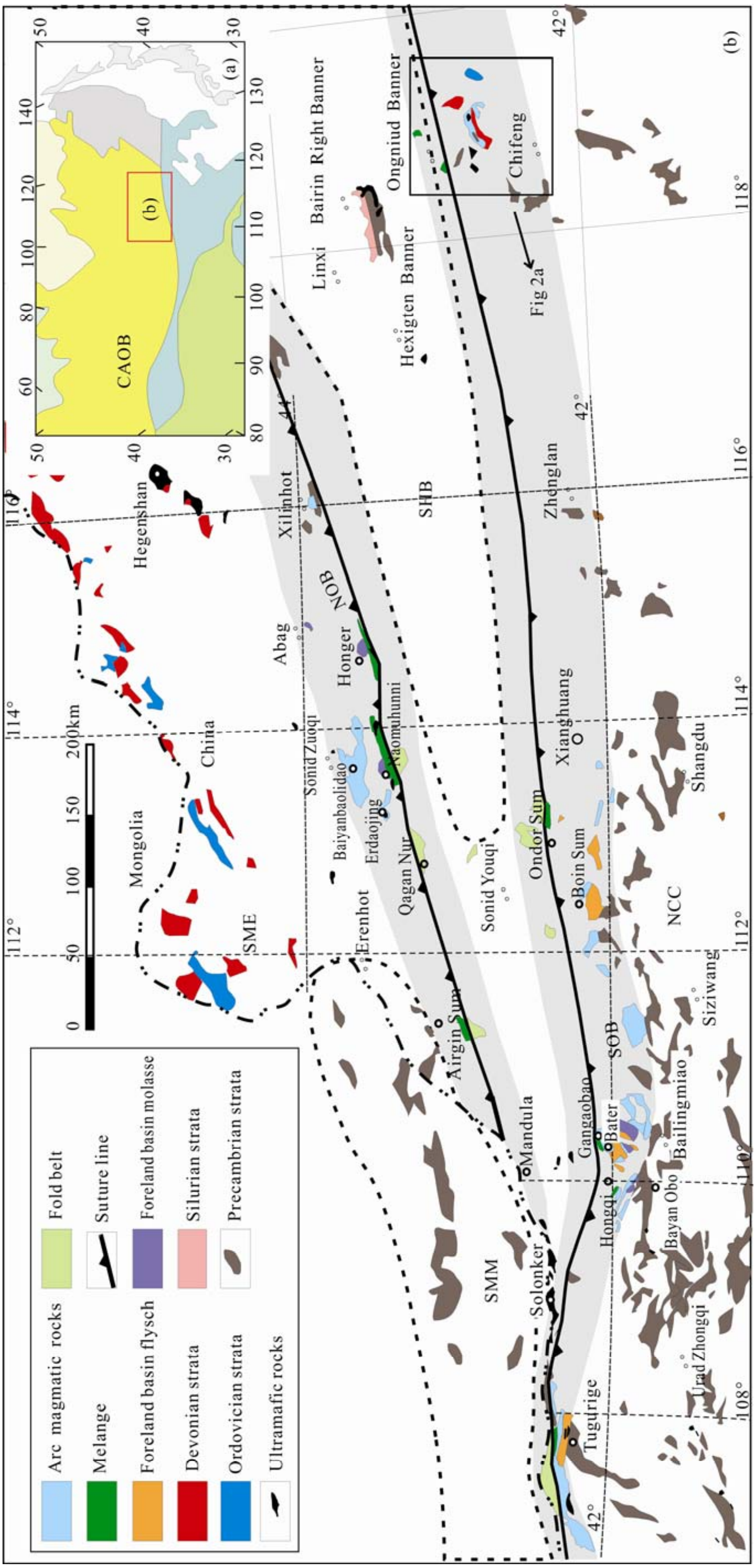

Fig. 1. (a) Simple tectonic map of the CAOB; (b) tectonic unit map of eastern Inner Mongolia emphasis on the Early and Middle Paleozoic outcrops and Precambrian blocks (compiled from Shao, 1991; IMBGMR, 1991; Jian et al., 2008; Yarmolyuk et al., 2008; Xu et al., 2013).

Xu et al., 2001; Zhang et al., 2010; Zhang et al., 2017).

The NOB and SOB represent a record of the evolution process of the CAOB in northeast China and Inner Mongolia. However, there are still some important issues to be solved. Especially, as the border between the NCC and CAOB, the eastward extension of the SOB remains poorly constrained. In this paper, we report our new research on the accretionary prism and island arc belt in Chifeng area, Inner Mongolia, which will provide some new evidence for the eastward extension of the SOB and tectonic evolution of the CAOB.

2 Tectonic Setting

Three tectonic units have been recognized in Chifeng area, Inner Mongolia, from north to south, including the Qiganmiao accretionary prism, Jiefangyingzi arc belt and Sidaozhangpeng molasse basin (Fig. 2a).

2.1 The Qiganmiao accretionary prism

The accretionary prism is discontinuously distributed from Qiganmiao to Beishan areas of Ongniud Bannar (Fig.2a), which is characterized by well-exposed mélange including various blocks and heterogeneously deformed matrix. In Qiganmiao area, the largest outcrop can be sized up to 2 km × 4 km (Fig.2b), where the matrix, in fault relationship with the blocks (Fig. 3a, 3b), consists of marble and shows a highly penetrative deformation with northeast dipping foliations (Fig. 3c). The blocks range from 200 m to 500 m in size (Fig. 2b) and include gabbro (Fig. 3b), two-mica quartz schist (Fig. 3d), gneissic granite (Fig. 3e) and basic volcanic rock (Fig. 3f).

2.2 The Jiefangyingzi arc belt

This belt consists of pluton complex and volcanic rocks and occurs in a wide area of ca.30×70 km (Fig. 2a). The pluton complex include granite-porphyry, granodiorite, monzogranite, quartz porphyry and aplite. The monzogranite intrudes into the Precambrian Baoyintu Group, which implies that the arc belt developed on an old block of the NCC rather than ocean crust of the PAO. Zircon dating result of the monzogranite gives an age of 419.3±9.2 Ma and geochemistry research indicates that it belongs to a part of active continental margin arc belt (Chen et al., 2017). The volcanic rocks include the Xibiehe and Badangshan Formations. The Xibiehe Formation consist of tuffaceous sandstones and mudstones, rhyolites, acidic volcanic tuffs (Fig. 4a). The Badangshan Formation is characterized by a sequence including volcanic breccia, interbedded tuff and rhyolite, and intermediate-basic volcanic rock, from low to up (Fig. 4b). With northwest dipping penetrative foliations, original thickness and sequence of these two Formations are not preserved because of strong deformation.

2.3 The Sidaozhangpeng molasse basin

Represented by the late Devonian Sidaozhangpeng Formation, the Sidaozhangpeng molasse basin can be traced from Sidaozhangpeng to Haladaokou areas, extending 80 Km in length (Fig. 2a). Due to later regional deformation, the rocks of Sidaozhangpeng Formation were sheared and compressed, but the original sequence can still be preserved (Fig. 5). Several sedimentary cycles with thickness of 20-40 meters have been recognized, which consist of conglomerates at the lower part and sandstones or siltstones at the upper part of the cycles. There are a lot of gravels of ancient metamorphic rocks and volcanic rocks in the conglomerates, which indicates they came from the NCC with old basement and the Jiefangyingzi arc belt, respectively. Generally, the sequence of Sidaozhangpeng molasse basin is characterized by proximity, coarseness and large thickness, similar to the proximity molasses basin. (Xia et al., 1989).

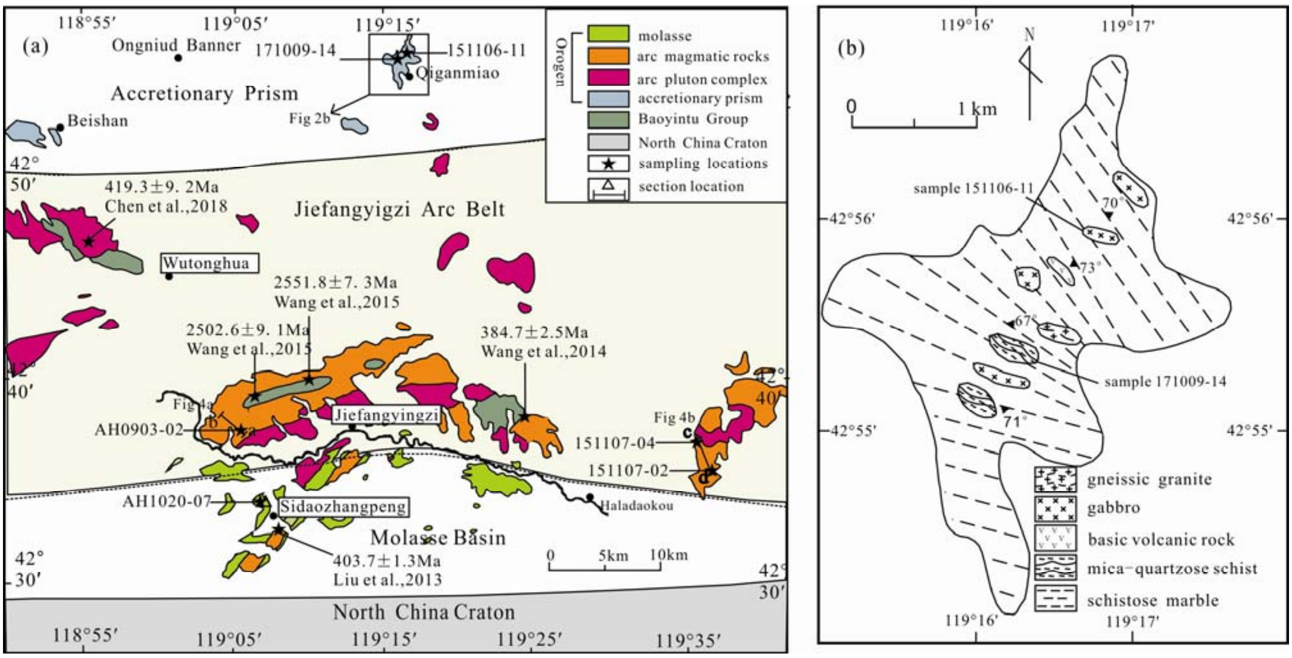

Fig. 2. (a) The early-middle Paleozoic tectonic unit map of the Chifeng-Ongniud area; (b) distribution map of mélange in the Qiganmiao area.

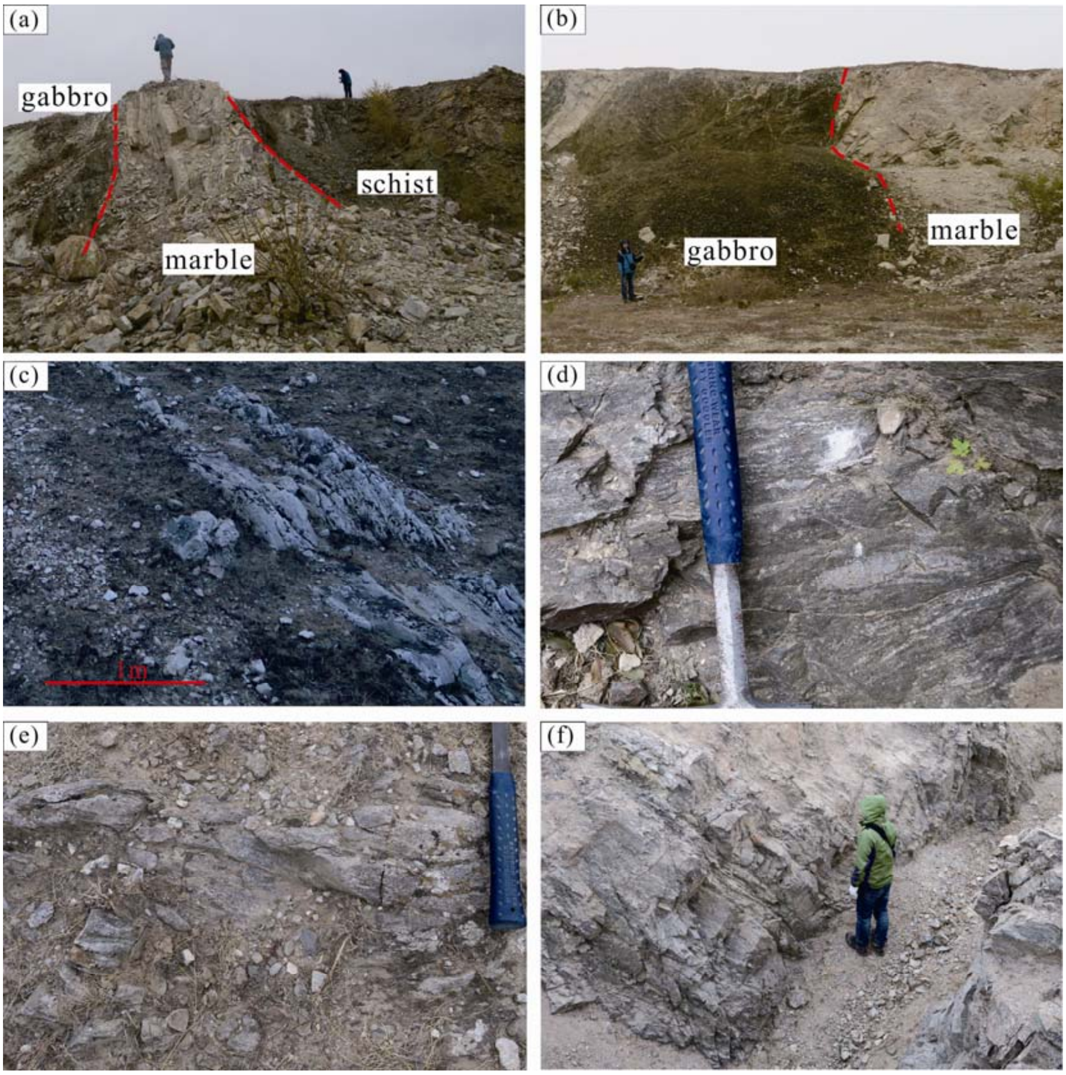

Fig. 3. Field sections of melange.
(a) fault relation between marble (matrix) and two-mica quartz schist (block); (b) fault relation between marble (matrix) and gabbro (block); (c) penetrative schistosity in matrix; (d) two-mica quartz schist block; (e) gneissic granite block; (f) volcanic rock block.

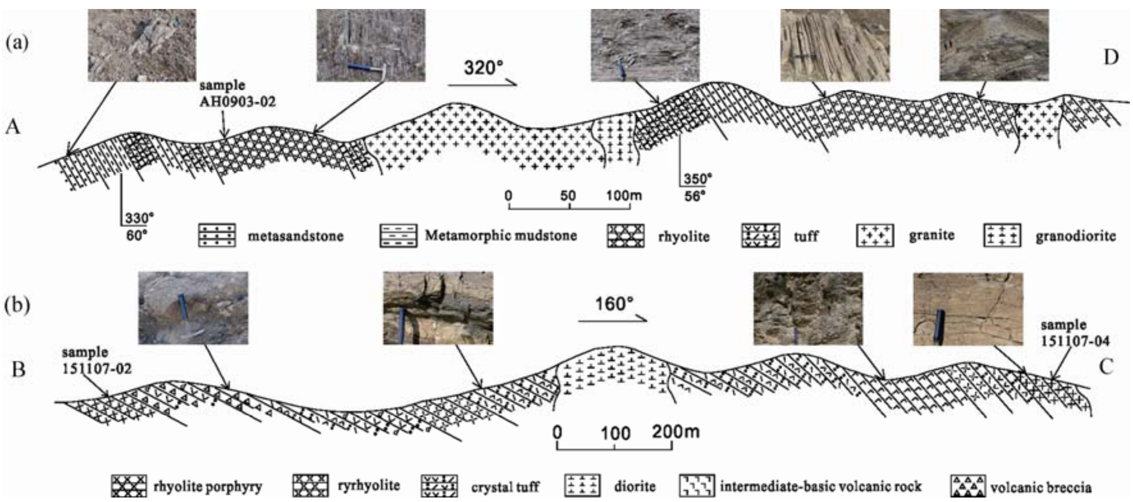

Fig. 4. (a) Field section of the Xibiehe Formation; (b) field section of the Badangshan Formation.

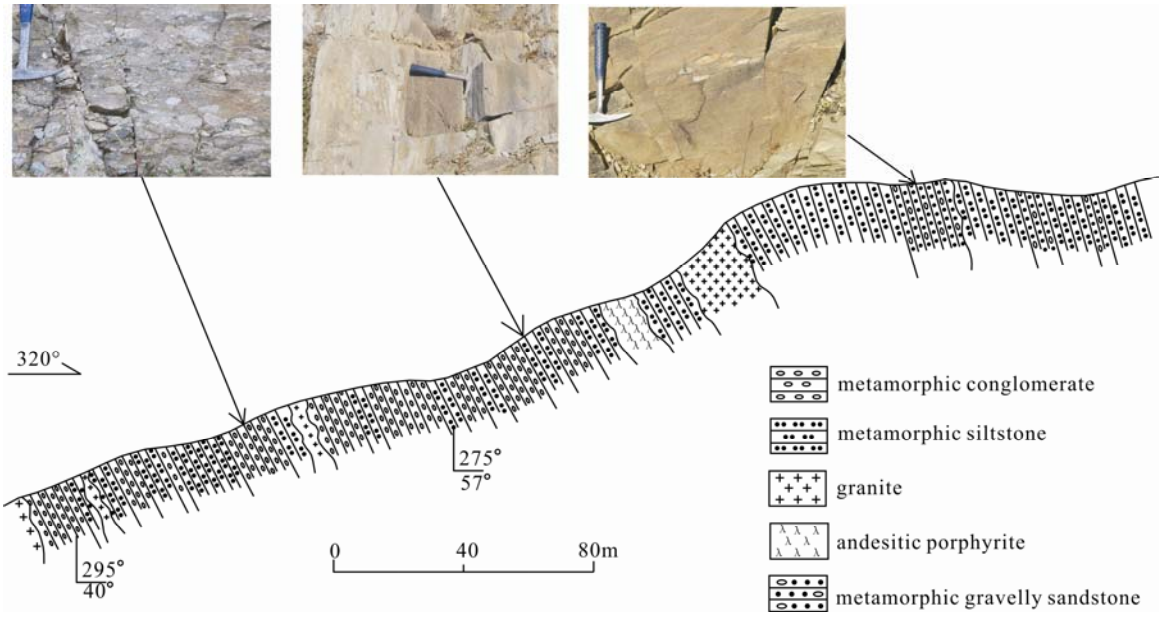

Fig. 5. Field section of the Sidaozhangpeng Formation.

3 Sample and Analytical Methods

3.1 Samples

In this study, eighteen rocks including gabbro, two-mica quartz schist, andesite and rhyolitic porphyry were sampled for petrographic, geochronological and geochemical analyses.

The gabbro in outcrop are fresh, show gabbroic textures (Fig. 6a) and massive structure. In thin section, they are fine grained, and composed of plagioclase (40–50%), clinopyroxene (~50%) and amphibole (~5%), with accessory sphene and Fe-Ti oxides (magnetite and ilmenite). Clinopyroxene crystals are subhedral to anhedral, and range in size from 0.2 mm to 0.5 mm (Fig. 6a). Plagioclase crystals are subhedral to anhedral, range in size from 0.1 mm to 0.5 mm, but some grains are partially altered to saussurite and sericite (Fig. 6a).

The two-mica quartz schist mainly consists of quartz (20–25%), plagioclase (~20%), biotite (~40%) and muscovite (~15%), with schistosity structure (Fig. 6b). Quartz crystals are anhedral, and range in size from 0.05 mm to 0.15 mm (Fig. 6b), and plagioclase crystals are subhedral and range in size from 0.05 mm to 0.2 mm (Fig. 6d). Both biotite and muscovite are anhedral and range in size from 0.05 mm to 0.2 mm (Fig. 6b).

The rhyolitic porphyry are characterized by a porphyritic texture (Fig. 6c and d). Small quantity of phenocrysts is mainly quartz and plagioclase, with lengths of 0.1 mm to 0.5 mm. Some of the quartz phenocrysts show wavy extinction. The plagioclase phenocrysts have polycrystalline twins, and some are altered (Fig. 6c). The groundmass of these volcanic rocks is mostly quartz and plagioclase.

3.2 Zircon cathodoluminescence (CL) imaging and U–Pb isotopic dating

Five samples including 171009-14, 151106-11, AH0903-02, 151107-02 and 151107-04 were choosed for zircon U–Pb isotopic dating. Zircons were separated using conventional heavy liquid and magnetic techniques and further separated by handpicking under a binocular microscope at the Langfang Regional Geological Survey, Hebei Province, China. Handpicked zircons were photographed under transmitted and reflected light under optical microscope and subsequently cathodoluminescence (CL) imaged using a Quanta 200 FEG Scanning Electron Microscope at Peking University. The CL images reveal the internal textures and potential target sites for U-Pb analyses.

The U-Pb zircon dating was carried out by an Agilient 7500c ICP-MS instrument coupled with a 193-nm ArF Excimer laser ablation system at the Key Laboratory of Orogeny and Crust Evolution, Peking University. Denudation was taken under a designed condition with 32 μm laser beam spot, 10 j/cm^2 laser energy density and 5 Hz frequency. U-Pb zircon ages were corrected using zircon Plesovice (337 Ma) as an external standard (Sláma et al., 2008) and zircon standard 91500 as a secondary standard to identify any deviation in age measurements. Concentration calibrations were carried out using NIST 610 glass as an external standard and Si as internal standard. Isotopic ratios and element concentrations of zircons were calculated using GLITTER (ver. 4.4.2, Macquarie University). Concordia ages and diagrams were obtained using Isoplot/Ex (3.0) (Ludwig, 2003). The common lead was corrected using LA-ICP-MS Common Lead Correction (ver. 3.15), following the method of Andersen (2002). The analytical data are presented on U-Pb Concordia diagrams with 2σ errors. The mean ages are weighted means with 95% confidence levels (Ludwig, 2003).

3.3 Major and trace element geochemistry

Major elements were analyzed by X-ray fluorescence

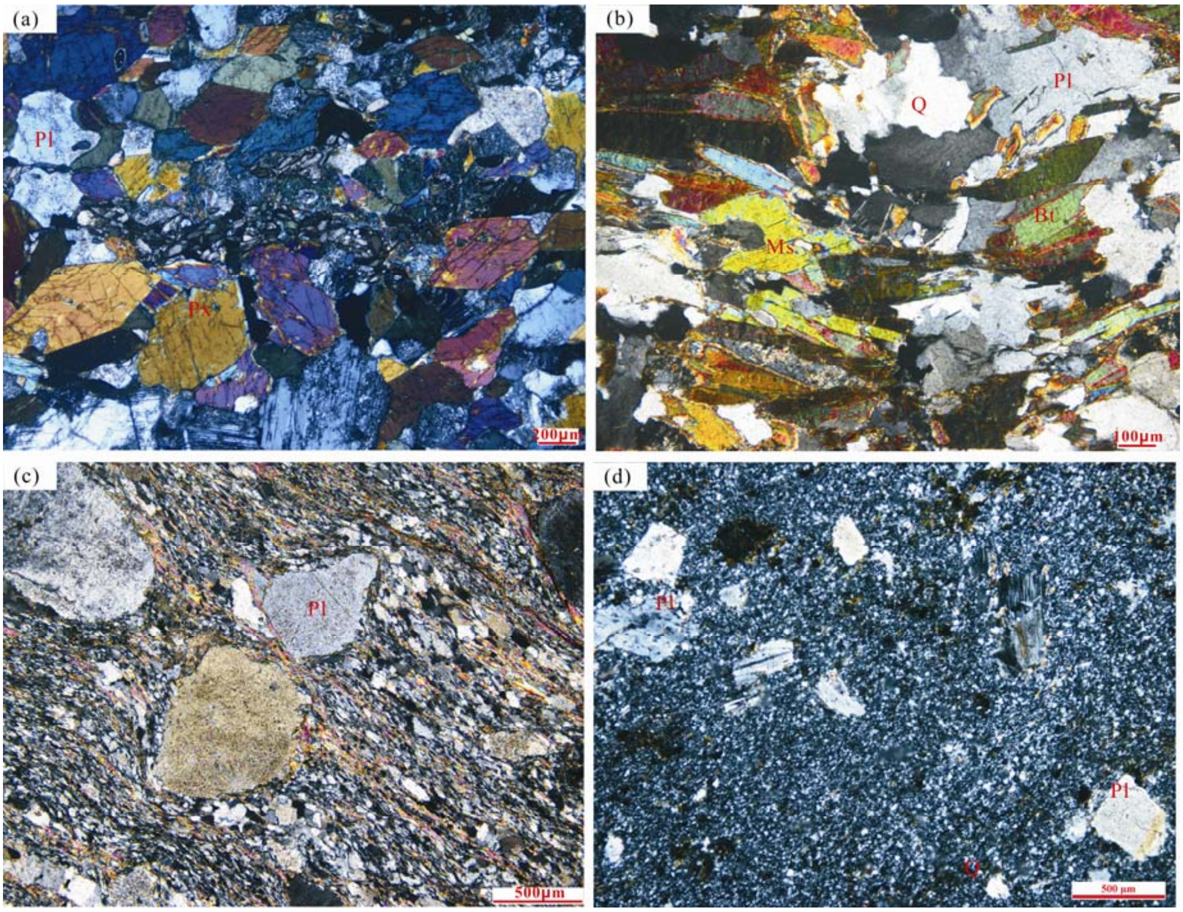

Fig. 6. Microscopic photos of zircon chronological samples. (a) gabbro; (b) two-mica schist; (c, d) ryholitic porphyry. Px-Pyroxene; Bt-Biotite; Ms-Muscovite; Pl-Plagioclase; Q=Quartz.

(XRF) at the Key Laboratory of Orogeny and Crust Evolution, Peking University, China. The analysis used fused glass disks on ARL ADVANT' XP+ with 50 kV accelerating voltage and 50 mA accelerating current. Analytical error was limited to 1% monitored by Chinese national standard samples GSR-1 and GSR-3.

The determination of trace element and rare earth elements (REEs) samples was carried out at the Key Laboratory of Orogenic Belts and Crustal Evolution, Peking University with an ELEMENT-1 plasmamass spectrometer (Finnigan-MAT Ltd.). The details of the sample preprocessing procedures can be found in Deng et al. (2014).

4 Analytical Results

4.1 Zircon morphology and U–Pb ages

The zircon CL images are shown in Fig. 7. The LA–ICP–MS zircon U–Pb isotopic dating results are listed in Table 1, and the concordia diagrams are presented in Fig. 8.

Sample 151106-11, a gabbro, was collected from the Qiganmiao accretionary prism. The zircons are anhedral in shape, without zoning internal structure. We conducted U–Pb isotopic dating in twenty nine spots on zircons and twenty four of them are concordant and can be divided into two groups. The older one, with Th/U ratios of 0.02–1.06, yields a weighted mean $^{206}Pb/^{238}U$ age of 492±3 Ma (MSWD=0.099, n=18). The young one, ranged in age from 441 Ma to 449 Ma，with Th/U ratios of 0.03–0.52, yields a weighted mean $^{206}Pb/^{238}U$ age of 446±6 Ma (Fig. 8a, MSWD=0.025, n=6). Because of zircon morphology (without zoning internal structure, Wu et al., 2004) and low Th/U ratios (some of them are 0.02-0.05), the young group should represent a meatmorphic age of the gabbro, whereas the older ages are interpreted as the ages of inherited or captured zircons.

Sample 171009-14, a two-mica quartz schist, was also collected from the Qiganmiao accretionary prism. Its zircon grains are prismatic and vary in lengths from 20 μm to 100 μm (Fig. 7). The CL images indicate that the zircons have obvious cores and metamorphic newborn rims, and some cores show oscillatory zoning. Besides two isolated zircons of 521±5 and 782±7 Ma, the other detrital zircons have concordant ages ranging from 1099±18 Ma to 2254±35 Ma(Fig. 8d). Ages of the youngest zircon group are between 1099±18 Ma and 1114±25 Ma, with a weighted mean age of 1104±27 Ma (n=4), which constrains the youngest depositional age of the protolith of the schist (Fig. 8c).

Sample AH0903-02, a rhyolite, was collected from the upper member of the Xibiehe Formation. The majority of zircons from the sample is euhedral–subhedral and shows oscillatory zoning, which indicates a magmatic origin.

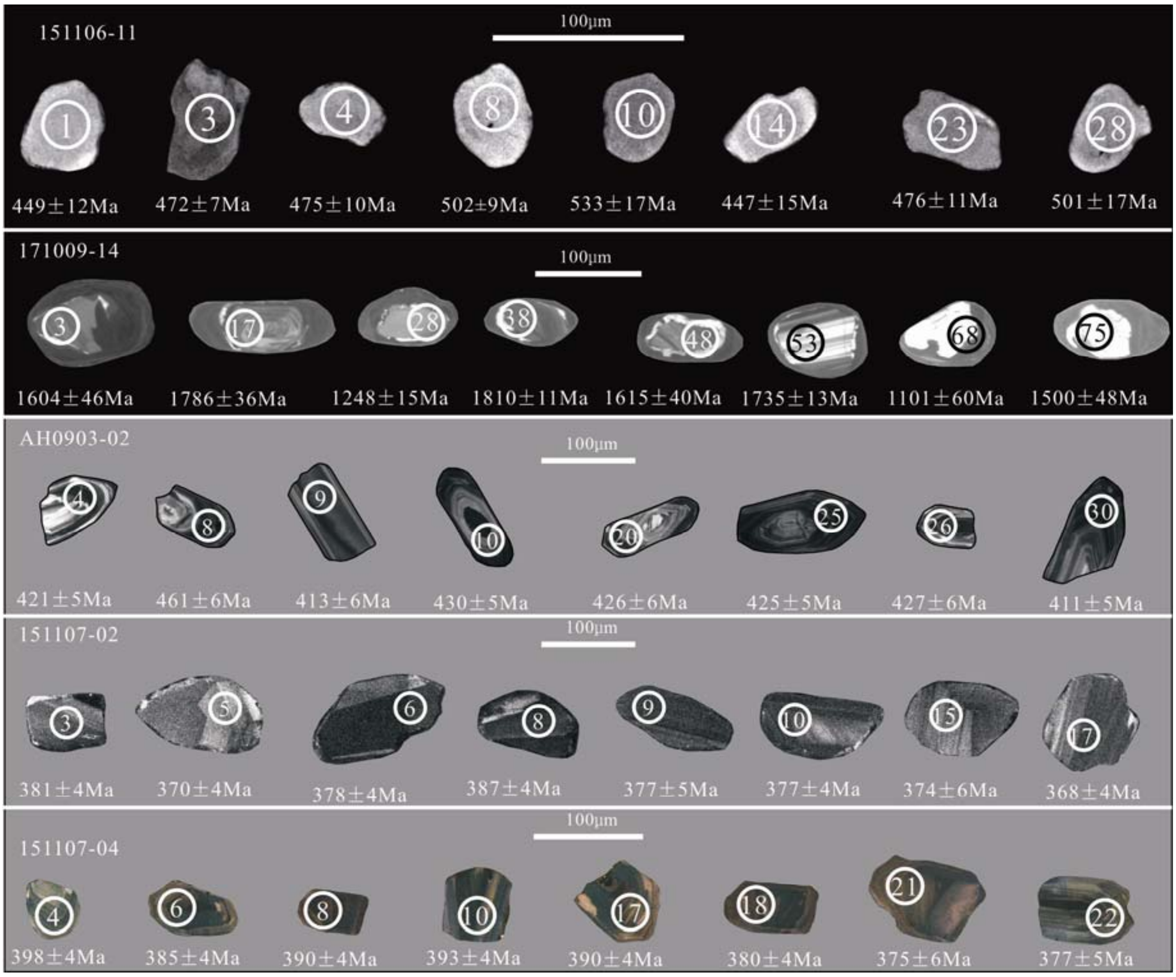

Fig. 7. Cathodoluminescence (CL) images and U–Pb zircon ages of selected zircons from the Early–Middle Paleozoic igneous and metamorphic rock of Chifeng area. White and balck circles represent the analyzed locations of zircon age, and the values below the images show zircon dating results.

Their Th/U ratios range from 0.03 to 2.33. Fifteen analyses yield a weighted mean $^{206}Pb/^{238}U$ age of 415±6 Ma, representing the crystallization age of the rhyolite (Fig.8b).

Samples of rhyolitic porphyry (151107-02 and 151107-04) are from the middle and lower parts of the Badansghan Formation, respectively. Zircons of sample 151107-02 are euhedral–subhedral and display striped absorption (Fig. 7), indicating a magmatic origin. The weighted mean $^{206}Pb/^{238}U$ age of 378.3±2.6 Ma (MSWD=1.7, n=19) indicates that the rhyolitic porphyry crystallized in the Late Devonian. The analyzed zircon grains of sample 151107-04 display subhedral crystal morphologies and oscillatory zoning, indicating a magmatic origin. Twenty analyses yield two weighted mean $^{206}Pb/^{238}U$ ages of 399±4 Ma and 383.2±3.4 Ma, the younger age is interpreted as crystallization age of the rhyolitic porphyry (Fig. 8f).

4.2 Whole-rock major and trace elemental geochemistry

Analysis results of major and trace elements are presented in Table 2.

4.2.1 Major and trace element compositions of the Xibiehe Formation

The rhyolite of the Xibiehe formation has variable SiO_2 contents ranging from 61.80 to 76.47 wt% and low K_2O+Na_2O contents ranging from 4.21 to 6.60 wt%, respectively. On the SiO_2 vs. Na_2O+K_2O (TAS) diagram (Fig. 9a), all the samples plot in the granodiorite field, with subalkaline compositions. On the SiO_2 vs. K_2O diagram, the samples fall into the middle-K to high-K calc -alkaline series (Fig. 9b). Besides, the rhyolite have high content of Al_2O_3 (10.57 wt%–17.30 wt%), and the A/CNK (molar Al_2O_3/CaO+K_2O) ratios of the samples vary between 0.95 and 1.28 (mean value of 1.19), showing a Peraluminous signature (Fig. 9c).

Samples from the Xibiehe formation have total REE contents (ΣREE) ranging from 141.24 ppm to 209.58 ppm. On chondrite-normalized REE diagrams (Fig. 10b), they display slight light REE enrichment (La_N/Yb_N = 11.32–12.64) and have slight negative Eu anomalies (Eu/Eu* = 0.68–0.76). On the primitive mantle-normalized multielement diagram (Fig. 10a), the samples display a strong depletion of high field strength elements (HFSEs; e.g., Nb and Ta) and enrich of large ion lithophile

Table 1 Zircon LA-ICP-MS isotopic data of the Chifeng area

spot	Th (ppm)	U (ppm)	Th/U	Isotopic ratio $^{207}Pb/^{206}Pb$ ratio	1σ	$^{207}Pb/^{235}U$ ratio	1σ	$^{206}Pb/^{238}U$ ration	1σ	Age(Ma) $^{207}Pb/^{206}Pb$ age	1σ	$^{207}Pb/^{235}U$ age	1σ	$^{206}Pb/^{238}U$ age	1σ	Unconcordance (%)
151106-11																
1	1.59	34.96	0.05	0.05308	0.0093	0.52744	0.09165	0.07206	0.00201	332	320	430	61	449	12	–4.23
2	0.17	5.70	0.03	0.05822	0.05332	0.5754	0.52483	0.07167	0.00656	538	1215	462	338	446	39	3.59
3	25.50	133.28	0.19	0.05613	0.00322	0.58852	0.03309	0.07604	0.00116	458	98	470	21	472	7	–0.42
4	32.19	48.89	0.66	0.05769	0.00632	0.60868	0.06597	0.07651	0.00159	518	205	483	42	475	10	1.68
5	19.83	28.22	0.70	0.05655	0.01883	0.64691	0.21376	0.08296	0.00443	474	538	507	132	514	26	–1.36
6	4.91	16.91	0.29	0.05746	0.0198	0.62047	0.21281	0.07832	0.00312	509	587	490	133	486	19	0.82
8	62.32	81.01	0.77	0.06119	0.00462	0.68393	0.05086	0.08106	0.00143	646	130	529	31	502	9	5.38
9	1.44	6.47	0.22	0.05511	0.04149	0.55991	0.41985	0.07369	0.00554	417	1091	451	273	458	33	–1.53
10	2.13	17.39	0.12	0.0581	0.01381	0.69009	0.16306	0.08615	0.00287	534	427	533	98	533	17	0.00
11	84.44	79.90	1.06	0.05989	0.00399	0.67731	0.04433	0.08202	0.00137	600	113	525	27	508	8	3.35
12	4.42	11.89	0.37	0.05741	0.02384	0.61012	0.25239	0.07708	0.00333	507	708	484	159	479	20	1.04
14	10.22	25.66	0.40	0.06101	0.01368	0.60422	0.13435	0.07184	0.00252	640	413	480	85	447	15	7.38
15	0.77	27.71	0.03	0.05929	0.02253	0.73822	0.2792	0.09032	0.00399	578	656	561	163	557	24	0.72
16	0.31	7.47	0.04	0.05714	0.04411	0.56537	0.43454	0.07178	0.00596	497	1137	455	282	447	36	1.79
18	0.65	7.83	0.08	0.05867	0.02797	0.67649	0.32085	0.08365	0.00474	555	820	525	194	518	28	1.35
19	2.79	8.58	0.33	0.06017	0.04498	0.58684	0.43673	0.07075	0.0054	610	1129	469	279	441	33	6.35
20	29.54	93.92	0.31	0.05561	0.00335	0.62441	0.03699	0.08147	0.0013	437	104	493	23	505	8	–2.38
21	17.90	34.26	0.52	0.05689	0.00784	0.62493	0.08533	0.07971	0.00202	487	260	493	53	494	12	–0.20
22	13.35	28.02	0.48	0.06205	0.01597	0.63969	0.1636	0.07481	0.00245	676	475	502	101	465	15	7.96
23	17.89	36.78	0.49	0.0554	0.00723	0.58506	0.07551	0.07663	0.00188	428	246	468	48	476	11	–1.68
24	0.31	13.45	0.02	0.05861	0.02286	0.65081	0.25199	0.08058	0.00477	553	642	509	155	500	28	1.80
26	0.66	5.24	0.13	0.05706	0.05537	0.70934	0.68579	0.09023	0.00832	494	1259	544	407	557	49	–2.33
27	16.94	32.85	0.52	0.05497	0.00971	0.53993	0.0947	0.07129	0.00181	411	336	438	62	444	11	–1.35
28	4.36	18.95	0.23	0.05697	0.01482	0.63456	0.16408	0.08085	0.00287	490	449	499	102	501	17	–0.40
171009-14																
1	96.30	170.02	0.57	0.10989	0.00238	4.69973	0.08982	0.31019	0.00316	1798	40	1767	16	1742	16	3.21
2	264.88	555.75	0.48	0.10313	0.0021	4.04084	0.07212	0.28418	0.0028	1681	39	1642	15	1612	14	4.28
3	163.08	243.94	0.67	0.09892	0.0024	3.80604	0.08354	0.27904	0.00288	1604	46	1594	18	1587	14	1.07
4	21.31	402.76	0.05	0.07629	0.00152	1.76105	0.03031	0.16741	0.00167	1103	41	1031	11	998	9	3.31
6	126.57	214.00	0.59	0.10974	0.00256	4.52696	0.09419	0.29918	0.00316	1795	43	1736	17	1687	16	6.4
7	51.37	131.13	0.39	0.1052	0.00214	4.38373	0.07717	0.30223	0.00306	1718	38	1709	15	1702	15	0.94
9	199.23	303.44	0.66	0.09391	0.00232	3.28532	0.07394	0.25373	0.0026	1506	48	1478	18	1458	13	3.29
10	187.50	441.77	0.42	0.10513	0.00203	4.19342	0.06998	0.2893	0.00279	1717	36	1673	14	1638	14	4.82
11	114.12	376.48	0.30	0.10155	0.00191	3.88946	0.06256	0.2778	0.00273	1653	36	1611	13	1580	14	4.62
12	51.38	157.78	0.33	0.07674	0.00176	1.63828	0.03584	0.15481	0.00187	1114	25	985	14	928	10	6.14
13	34.49	431.40	0.08	0.10857	0.00149	4.71388	0.06007	0.31483	0.00306	1776	11	1770	11	1764	15	0.68
16	90.72	399.92	0.23	0.10343	0.00172	4.05633	0.05591	0.28445	0.00267	1687	31	1646	11	1614	13	4.52
17	109.23	264.65	0.41	0.10918	0.00212	4.68845	0.07837	0.31146	0.00305	1786	36	1765	14	1748	15	2.17
18	68.32	152.89	0.45	0.10396	0.00224	4.01477	0.07637	0.28009	0.00285	1696	41	1637	15	1592	14	6.53
19	115.43	339.79	0.34	0.09386	0.00179	3.19528	0.05257	0.24689	0.00238	1505	37	1456	13	1422	12	5.84
20	159.83	112.26	1.42	0.10669	0.00158	4.32078	0.05996	0.29368	0.00297	1744	12	1697	11	1660	15	5.06
23	55.06	396.75	0.14	0.10066	0.00162	3.7628	0.04953	0.27112	0.00253	1636	31	1585	11	1547	13	5.75
24	146.33	422.26	0.35	0.10425	0.00191	3.94234	0.06143	0.27426	0.00262	1701	34	1622	13	1562	13	8.9
25	236.26	429.63	0.55	0.10126	0.00216	3.83219	0.07251	0.27447	0.0027	1647	40	1600	15	1563	14	5.37
27	214.89	237.48	0.90	0.11326	0.00299	5.22898	0.12644	0.33484	0.00355	1852	49	1857	21	1862	17	–0.54
28	125.35	134.68	0.93	0.08209	0.00132	2.34797	0.03566	0.20742	0.0021	1248	15	1227	11	1215	11	2.72
29	196.26	411.09	0.48	0.08388	0.00229	2.53672	0.06398	0.21935	0.0023	1290	54	1283	18	1278	12	0.94
31	167.57	285.31	0.59	0.08391	0.00122	2.32529	0.0316	0.20096	0.00195	1290	13	1220	10	1180	10	9.32
32	90.50	236.76	0.38	0.10386	0.00204	4.26148	0.07251	0.29758	0.00293	1694	37	1686	14	1679	15	0.89
33	42.57	88.37	0.48	0.08934	0.00151	2.98679	0.04792	0.24244	0.00255	1411	16	1404	12	1399	13	0.86
34	167.55	339.40	0.49	0.10842	0.00222	4.49631	0.08059	0.30079	0.00297	1773	38	1730	15	1695	15	4.6
36	156.42	176.44	0.89	0.10183	0.00156	3.86286	0.05554	0.2751	0.00279	1658	13	1606	12	1567	14	5.81
37	83.37	275.49	0.30	0.10422	0.00203	3.92056	0.06556	0.27284	0.0027	1701	37	1618	14	1555	14	9.39
38	103.74	390.89	0.27	0.11067	0.00151	4.77554	0.06047	0.31293	0.00298	1810	11	1781	11	1755	15	3.13
41	131.18	255.36	0.51	0.14223	0.00279	7.62598	0.12828	0.38888	0.00391	2254	35	2188	15	2118	18	6.42
42	56.41	452.53	0.12	0.06923	0.00149	1.2311	0.02359	0.12898	0.00126	906	45	815	11	782	7	4.22
43	54.10	255.74	0.21	0.10352	0.00187	4.13622	0.06285	0.2898	0.00281	1688	34	1661	12	1641	14	2.86
44	30.41	331.10	0.09	0.1118	0.00157	5.10147	0.06666	0.33091	0.00319	1829	11	1836	11	1843	15	–0.76
45	191.41	284.38	0.67	0.11237	0.00159	5.0336	0.06645	0.32483	0.00315	1838	11	1825	11	1813	15	1.38
46	179.45	226.45	0.79	0.11122	0.00161	5.04213	0.06804	0.32875	0.00322	1819	12	1826	11	1832	16	–0.71
48	81.67	224.02	0.36	0.0995	0.0021	3.56331	0.06603	0.25974	0.00262	1615	40	1541	15	1489	13	8.46
49	51.30	263.38	0.19	0.10379	0.00187	4.1087	0.06217	0.28711	0.00279	1693	34	1656	12	1627	14	4.06
50	51.47	143.01	0.36	0.10641	0.00262	4.14817	0.09134	0.28273	0.00312	1739	46	1664	18	1605	16	8.35
51	446.15	612.16	0.73	0.09776	0.00262	3.8402	0.09507	0.28489	0.00294	1582	51	1601	20	1616	15	–2.1
52	107.56	214.65	0.50	0.10398	0.0024	4.09991	0.08491	0.28597	0.00294	1696	44	1654	17	1621	15	4.63
53	101.02	158.96	0.64	0.10619	0.00162	4.84797	0.06932	0.33107	0.00332	1735	13	1793	12	1844	16	–5.91
54	75.40	109.10	0.69	0.10854	0.00172	4.98295	0.07471	0.33293	0.00344	1775	14	1816	13	1853	17	–4.21
56	358.20	659.63	0.54	0.10626	0.00237	4.06767	0.08109	0.27764	0.00278	1736	42	1648	16	1579	14	9.94

Contiuned Table 1

spot	Th	U	Th/U	Isotopic ratio						Age(Ma)						Unconcordance (%)
				$^{207}Pb/^{206}Pb$		$^{207}Pb/^{235}U$		$^{206}Pb/^{238}U$		$^{207}Pb/^{206}Pb$		$^{207}Pb/^{235}U$		$^{206}Pb/^{238}U$		
	(ppm)	(ppm)		ratio	1σ	ratio	1σ	ration	1σ	age	1σ	age	1σ	age	1σ	
57	87.27	143.28	0.61	0.09429	0.00273	3.23651	0.08676	0.24896	0.00272	1514	56	1466	21	1433	14	5.65
60	104.72	130.56	0.80	0.09046	0.00325	3.10975	0.10563	0.24931	0.0029	1435	70	1435	26	1435	15	0
61	72.90	367.15	0.20	0.10819	0.00197	4.57626	0.07053	0.30678	0.003	1769	34	1745	13	1725	15	2.55
62	41.96	189.29	0.22	0.07616	0.00136	1.50856	0.02539	0.14364	0.00149	1099	18	934	10	865	8	7.98
65	25.31	227.49	0.11	0.10734	0.00168	4.16369	0.0612	0.2813	0.00282	1755	13	1667	12	1598	14	9.82
67	44.69	98.50	0.45	0.09936	0.00253	3.9286	0.09026	0.28676	0.00314	1612	49	1620	19	1625	16	–0.8
68	73.16	206.90	0.35	0.07622	0.00224	1.89198	0.05193	0.18004	0.00192	1101	60	1078	18	1067	11	3.19
69	151.95	175.66	0.87	0.10443	0.00169	3.97166	0.06065	0.27581	0.00282	1704	14	1628	12	1570	14	8.54
70	91.46	208.88	0.44	0.10967	0.00175	4.36341	0.06552	0.28854	0.00292	1794	14	1705	12	1634	15	9.79
71	11.37	919.70	0.01	0.0578	0.00096	0.67094	0.01045	0.08419	0.00084	522	18	521	6	521	5	0
72	101.06	511.66	0.20	0.09704	0.00189	3.6536	0.0615	0.27307	0.0027	1568	37	1561	13	1556	14	0.77
74	121.55	166.22	0.73	0.10351	0.0032	4.10667	0.11825	0.28774	0.00323	1688	58	1656	24	1630	16	3.56
75	112.87	274.73	0.41	0.0936	0.00232	3.28194	0.07363	0.25431	0.00265	1500	48	1477	17	1461	14	2.67
151107-02																
1	162.87	119.81	1.36	0.05416	0.0021	0.45643	0.01725	0.06112	0.00072	378	64	382	12	382	4	0.00
2	64.21	62.57	1.03	0.05181	0.00324	0.42749	0.02631	0.05983	0.00082	277	116	361	19	375	5	–3.73
3	107.69	94.86	1.14	0.05419	0.00235	0.45476	0.0193	0.06086	0.00074	379	74	381	13	381	4	0.00
4	218.75	148.25	1.48	0.05419	0.00188	0.45121	0.0152	0.06038	0.00068	379	55	378	11	378	4	0.00
5	168.30	129.07	1.30	0.05476	0.00205	0.44622	0.01625	0.05909	0.00068	402	61	375	11	370	4	1.35
6	323.08	245.04	1.32	0.05415	0.00153	0.45026	0.01229	0.06031	0.00064	377	42	377	9	378	4	–0.26
7	274.81	173.61	1.58	0.05313	0.00173	0.43637	0.01377	0.05957	0.00066	334	51	368	10	373	4	–1.34
8	191.64	155.99	1.23	0.05403	0.0018	0.46112	0.01496	0.0619	0.00069	372	53	385	10	387	4	–0.52
9	109.93	90.11	1.22	0.05668	0.0026	0.47094	0.02114	0.06026	0.00077	479	77	392	15	377	5	3.98
10	147.30	107.96	1.36	0.0557	0.00229	0.4626	0.01859	0.06023	0.00072	440	68	386	13	377	4	2.39
11	153.96	127.29	1.21	0.05362	0.00209	0.44732	0.01704	0.0605	0.00071	355	65	375	12	379	4	–1.06
12	101.80	88.71	1.15	0.05428	0.00255	0.45177	0.02078	0.06035	0.00076	383	81	379	15	378	5	0.26
13	317.17	191.83	1.65	0.0568	0.00179	0.47402	0.01448	0.06052	0.00067	484	48	394	10	379	4	3.96
14	339.41	184.57	1.84	0.05387	0.00172	0.45873	0.01425	0.06176	0.00068	366	50	383	10	386	4	–0.78
15	141.07	102.41	1.38	0.05215	0.00347	0.4301	0.02804	0.05981	0.00097	292	119	363	20	374	6	–2.94
16	107.33	85.76	1.25	0.05295	0.00275	0.43345	0.02208	0.05936	0.00076	327	93	366	16	372	5	–1.61
17	170.23	118.68	1.43	0.05461	0.00222	0.44244	0.01753	0.05876	0.0007	396	67	372	12	368	4	1.09
19	438.12	278.35	1.57	0.05315	0.00149	0.44799	0.01216	0.06112	0.00065	335	42	376	9	382	4	–1.57
20	239.94	166.93	1.44	0.05242	0.00204	0.44562	0.01694	0.06164	0.0007	304	66	374	12	386	4	–3.11
151107-04																
1	515.14	375.12	1.37	0.0561	0.00152	0.48348	0.01261	0.06251	0.00067	456	39	400	9	391	4	2.30
2	374.69	256.94	1.46	0.05464	0.00157	0.44511	0.01232	0.05909	0.00064	398	43	374	9	370	4	1.08
3	377.27	430.40	0.88	0.05711	0.00143	0.50189	0.01201	0.06374	0.00066	496	34	413	8	398	4	3.77
4	125.93	180.27	0.70	0.05559	0.0018	0.48767	0.01529	0.06363	0.00072	436	50	403	10	398	4	1.26
5	451.39	429.54	1.05	0.05681	0.00147	0.51041	0.01265	0.06517	0.00068	484	36	419	9	407	4	2.95
6	220.20	209.58	1.05	0.05418	0.0017	0.45966	0.01395	0.06153	0.00068	379	48	384	10	385	4	–0.26
7	70.95	125.98	0.56	0.05585	0.00299	0.47057	0.02453	0.06111	0.00075	446	122	392	17	382	5	2.62
8	540.06	363.98	1.48	0.05808	0.00161	0.49995	0.01332	0.06243	0.00066	533	40	412	9	390	4	5.64
9	764.81	413.60	1.85	0.05744	0.00167	0.50969	0.01423	0.06436	0.0007	508	42	418	10	402	4	3.98
10	280.76	246.45	1.14	0.05741	0.00171	0.49825	0.01429	0.06294	0.00069	507	44	411	10	393	4	4.58
11	160.99	184.34	0.87	0.04812	0.00626	0.38329	0.04955	0.05777	0.00082	105	262	329	36	362	5	–9.12
12	342.05	259.64	1.32	0.05576	0.00173	0.47031	0.01403	0.06117	0.00068	443	46	391	10	383	4	2.09
13	104.96	163.32	0.64	0.05652	0.00202	0.47118	0.01628	0.06047	0.0007	473	56	392	11	378	4	3.70
14	173.01	199.07	0.87	0.05546	0.00179	0.49008	0.01529	0.0641	0.00072	431	49	405	10	401	4	1.00
16	139.46	183.02	0.76	0.05461	0.00257	0.47037	0.02171	0.06248	0.00073	396	83	391	15	391	4	0.00
17	405.29	269.19	1.51	0.05646	0.00168	0.48504	0.01387	0.06231	0.00069	471	44	402	9	390	4	3.08
18	267.62	210.92	1.27	0.05498	0.00189	0.46031	0.01528	0.06073	0.0007	411	53	384	11	380	4	1.05
19	187.46	187.26	1.00	0.05709	0.00301	0.52228	0.02679	0.06635	0.00099	495	87	427	18	414	6	3.14
20	148.07	218.54	0.68	0.05409	0.00201	0.45117	0.01632	0.0605	0.0007	375	60	378	11	379	4	–0.26
21	157.63	197.62	0.80	0.05485	0.00302	0.4527	0.02424	0.05987	0.00091	406	93	379	17	375	6	1.07
22	124.83	216.99	0.58	0.05615	0.00228	0.4666	0.01835	0.06027	0.00077	458	64	389	13	377	5	3.18
23	43.83	61.87	0.71	0.05848	0.00327	0.48924	0.0268	0.06068	0.00085	548	95	404	18	380	5	6.32
24	457.57	282.88	1.62	0.05504	0.0018	0.48743	0.01542	0.06423	0.00072	414	51	403	11	401	4	0.50
25	719.39	446.61	1.61	0.05461	0.00177	0.42869	0.01337	0.05694	0.00065	396	49	362	10	357	4	1.40
AH0903-02																
1	77.76	857.59	0.09	0.49916	0.0121	0.06593	0.00082	0.01885	0.00108	412	32	411	8	412	5	–0.24
2	16.88	564.33	0.03	0.51153	0.01315	0.06733	0.00086	0.02538	0.0031	420	35	419	9	420	5	–0.24
3	262.96	574.15	0.46	0.51391	0.01632	0.06754	0.00094	0.02567	0.00092	423	46	421	11	421	6	0.00
4	58.58	591.52	0.10	0.55462	0.01485	0.06749	0.00088	0.02418	0.00139	592	36	448	10	421	5	6.41
5	14.70	339.81	0.04	0.68572	0.04074	0.08582	0.00145	0.09475	0.00949	531	101	530	25	531	9	–0.19
6	443.72	190.74	2.33	0.14348	0.01703	0.0214	0.00049	0.00775	0.00029	133	220	136	15	136	3	0.00
7	335.40	210.60	1.59	2.90378	0.06299	0.23919	0.00314	0.07195	0.00209	1386	22	1383	16	1382	16	0.29
8	312.49	537.22	0.58	0.57381	0.01605	0.0741	0.00095	0.02364	0.00077	462	39	460	10	461	6	–0.22
9	115.87	180.59	0.64	0.49998	0.02276	0.06613	0.00107	0.02044	0.00086	409	73	412	15	413	6	–0.24
10	320.10	445.06	0.72	0.52581	0.01442	0.06894	0.0009	0.02236	0.00072	428	38	429	10	430	5	–0.23

Contiuned Table 1

spot	Th	U	Th/U	Isotopic ratio						Age(Ma)						Unconcordance (%)
				$^{207}Pb/^{206}Pb$		$^{207}Pb/^{235}U$		$^{206}Pb/^{238}U$		$^{207}Pb/^{206}Pb$		$^{207}Pb/^{235}U$		$^{206}Pb/^{238}U$		
	(ppm)	(ppm)		ratio	1σ	ratio	1σ	ration	1σ	age	1σ	age	1σ	age	1σ	
11	353.77	559.46	0.63	0.13183	0.00702	0.01974	0.00033	0.00625	0.00028	124	90	126	6	126	2	0.00
12	716.69	564.05	1.27	0.44414	0.0169	0.05966	0.00084	0.01587	0.00053	374	60	373	12	374	5	–0.27
13	96.68	495.98	0.19	1.16982	0.03339	0.1228	0.0015	0.03732	0.00045	901	66	787	16	747	9	5.35
14	197.94	388.50	0.51	0.48477	0.03702	0.06433	0.00149	0.02121	0.00138	401	130	401	25	402	9	–0.25
15	114.27	258.33	0.44	0.85964	0.03183	0.10267	0.00162	0.03861	0.00164	632	53	630	17	630	9	0.00
16	109.21	134.41	0.81	0.29555	0.02587	0.04169	0.00077	0.01219	0.00068	262	165	263	20	263	5	0.00
17	183.60	465.95	0.39	0.47126	0.01843	0.06271	0.00097	0.01928	0.00092	395	60	392	13	392	6	0.00
19	84.33	312.65	0.27	2.04417	0.05487	0.18549	0.00229	0.05547	0.00064	1195	60	1130	18	1097	12	8.93
20	227.14	420.29	0.54	0.52084	0.0165	0.06836	0.00095	0.02196	0.00083	425	46	426	11	426	6	0.00
21	138.74	194.55	0.71	3.23021	0.11992	0.25057	0.00486	0.08334	0.00374	1500	41	1464	29	1441	25	4.09
22	115.06	482.34	0.24	0.59181	0.02487	0.07607	0.00105	0.02771	0.00157	471	68	472	16	473	6	–0.21
23	452.49	515.93	0.88	0.48591	0.0144	0.06436	0.00083	0.02036	0.00069	404	43	402	10	402	5	0.00
24	44.62	225.51	0.20	0.8998	0.0292	0.09861	0.00143	0.04935	0.00235	814	44	652	16	606	8	7.59
25	417.13	938.95	0.44	0.51922	0.01224	0.0682	0.00085	0.02168	0.00075	423	31	425	8	425	5	0.00
26	105.82	654.78	0.16	0.52179	0.0181	0.06841	0.00097	0.02554	0.00142	427	52	426	12	427	6	–0.23
27	255.39	421.70	0.61	0.55576	0.01698	0.07212	0.00099	0.02212	0.00086	450	44	449	11	449	6	0.00
29	249.75	439.99	0.57	0.48048	0.01287	0.06378	0.00082	0.02098	0.00075	399	37	398	9	399	5	–0.25
30	236.23	312.94	0.75	0.49805	0.0181	0.06577	0.00089	0.0206	0.00075	411	57	410	12	411	5	–0.24
31	314.40	1287.06	0.24	0.51805	0.0171	0.06801	0.00097	0.01929	0.001	424	48	424	11	424	6	0.00

elements (LILEs; e.g., Rb and Ba).

4.2.2 Major and trace element compositions of the Badangshan Formation

The basalts have a major element composition of SiO_2 =50.46–50.64 wt%, Al_2O_3 = 19.34–19.49 wt% and $Mg^{\#}$ = 51–53 [$Mg^{\#} = 100\ Mg^{2+}/(Mg^{2+}+Fe^{2+})$], as well as low K_2O (0.20–0.23 wt%) concentrations. In the total alkali vs silica (TAS) plot, all samples fall within the field of basalt and the sub-alkaline field (Fig. 9d). Additionally, the basalts also characterized by significant enrichments of large ion lithophile elements (LILEs; e.g., Ba and Sr) and depletion of high field strength elements (HFSEs; e.g., Nb and Ta), and there is basically no to slightly positive Eu anomalies on the primitive mantle-normalized multielement diagram (Eu/Eu* =1.06–1.11) (Fig. 10d) .

The Basaltic andesite belong to the alkali-calcic series and calc-alkaline series (Fig. 9e) and have SiO_2=54.10–55.82 wt%, Al_2O_3=16.45–17.07 wt%, total alkaline (K_2O+Na_2O) = 4.75–6.56 wt%, $Mg^{\#}$ = 41–46. They are enriched in light REEs (LREEs) and LILEs, Ba, Sr, and Rb, depleted in heavy REEs (HREEs) [$(La/Yb)_N$ = 3.02–4.08] and (HFSEs; e.g., Nb, Ta, Zr and Hf), and have no obvious Eu anomalies (Eu/Eu* = 1.00–1.08) (Fig. 10d).

Two samples of rhyolite belong to the calc-alkaline series (Fig. 9e) and have high SiO_2(73.11–74.87 wt%), high Al_2O_3(13.46–14.04 wt%), middle K_2O(0.22–0.76 wt%), high Na_2O(3.82–4.49 wt%) abundances, showing a Peraluminous signature(Fig. 9f). In the total alkali vs silica (TAS) plot, all samples plot in the field of sub-alkaline field (Fig. 9d). They display relatively enriched in light REEs, depleted in heavy REEs [$(La/Yb)_N$ = 6.64–7.39] and show obvious negative Eu anomalies (Eu/Eu* =0.40–0.51).

5 Discussion

5.1 Paleogeographic frame of the early-middle Paleozoic continental margin in Chifeng area

Previous research considered that the paleogeographic frame of the early-middle Paleozoic continental margin in Chifeng area is characterized by an arc-continent collision between the Ondor Sum-Ongniud Bannar island arc belt in the north and the NCC in the south (Li et al., 2009; Liu et al., 2013). However, the newly discovered mélange in Ongniud Bannar area in this study indicates that there was an accretionary prism rather than island arc belt there. Several newly published Precambrian ages, including of 2551.8±7.3 Ma (Wang et al., 2016), indicate that the northern continental margin of NCC extends to Jiefangyingzi area, where wide distribution of the early-middle Paleozoic volcanic rocks of the Badangshan and Xibiehe Formations and plutons suggests development of continental arc belt developed. It seems that the early-middle Paleozoic tectonic frame was not an arc-continent collision between the Ondor Sum-Ongniud Bannar island arc belt and NCC but the Andean-type subduction orogenic belt formed by the southward subduction of the Paleo Asian Ocean (PAO) under the northern continental margin of NCC in Chifeng area.

5.2 Development stages of the arc belt and its tectonic significance

The study of monzogranite in Wutonghua area, Ongniud Bannar shows that it belongs to active continental margin volcanic arc and give a forming age of 419.3±9.2 Ma (Chen et al., 2017). Liu et al. (2013) report an age of 403.7±1.3 Ma and Hf(t) values of -22.0–-16.4 of the volcanic rocks in the south of Jiefangyingzi area (Fig. 2a), and suggest they originated from partial melting of NCC. These ages are consistent with the age of 415±6 Ma from the Xibiehe Formation volcanic rock in this study, which implies that there was continent arc magmatism during 400–420 Ma in Chifeng area, and represents the first stage magmatic activity related to the subduction of the PAO. The rhyolites from the Xibiehe Formation belong to the subalkaline series, enriched LREE and LILE and depleted HFSE, with negative Eu anomalies, all of which suggest a continental arc-related setting. In general, the Nb vs. Y and Rb vs. (Y+Nb) diagrams are effective in

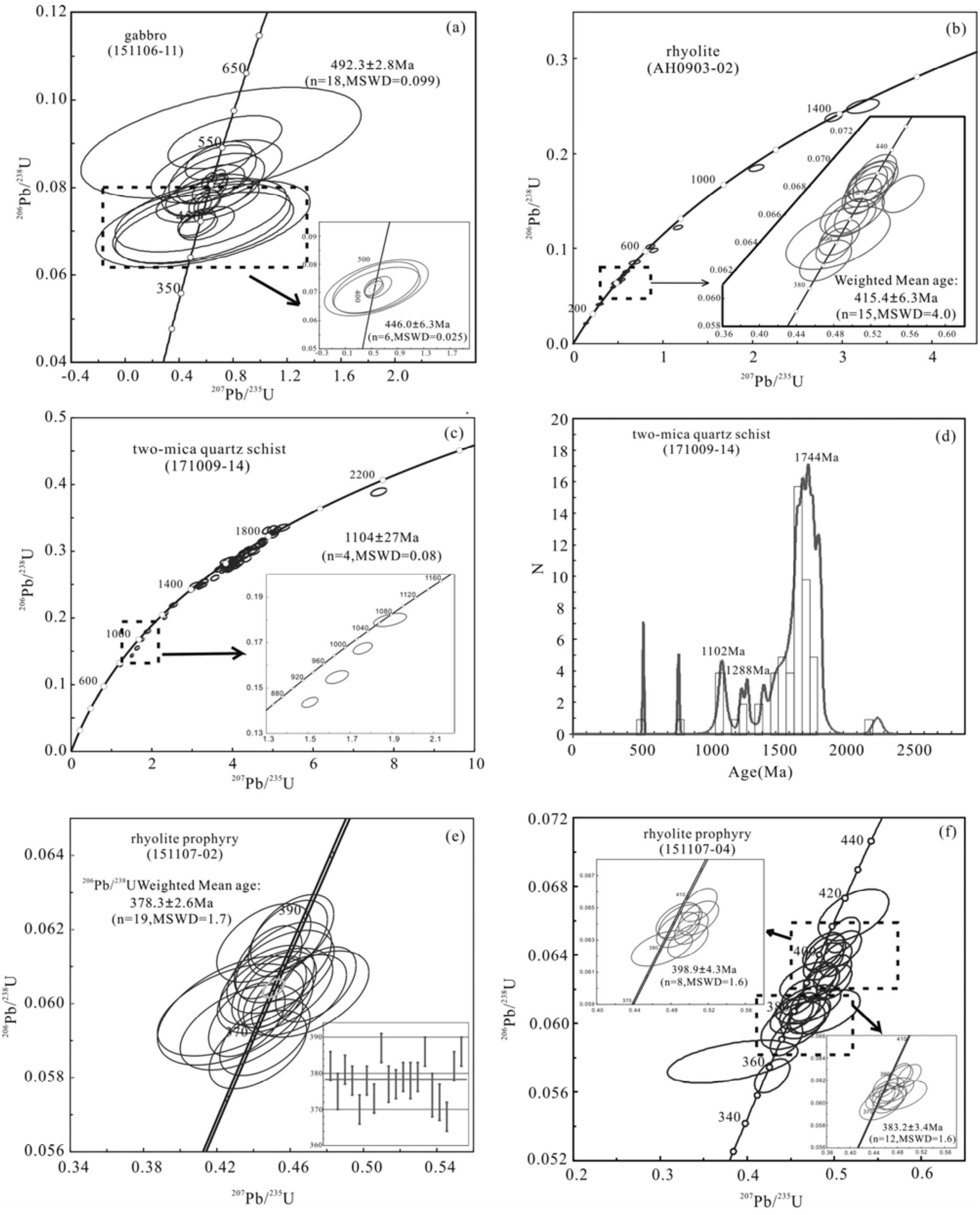

Fig. 8. Zircon U-Pb Concordia diagram and relative probability in Chifeng area.

discriminating the tectonic setting of granitoids (Pearce, 1996). The samples from the Xibiehe Formation plot in the volcanic arc field (Fig. 11a and b). This is also consistent with the Sr/Y vs. Y discrimination diagram (Fig. 11c). In summary, we propose that the granitoids of the Xibiehe Formation were potentially related to the continental arc-related setting.

The second phase magmatic activity occurred in 380-

Table 2 Major (wt%) and trace (ppm) element compositions of the Badangshan Formation and Xibiehe Formation

	Badangshan Formation							Xibiehe Formation					
	Rhyolite		Basalt		Basaltic andesite			Rhyolite	Andesite			Dacite	
Sample No.	171011-05a	171011-05b	171011-16b	171011-16d	171011-20b	171011-20c	171011-20d	171012-09a	171012-13a	171012-13b	171012-13e	171012-14	171012-15
Oxide composition (wt%)													
SiO_2	73.11	74.87	50.64	50.46	54.10	55.13	55.82	76.47	61.80	62.14	62.92	64.93	64.89
Al_2O_3	14.04	13.46	19.34	19.49	16.45	16.66	17.07	10.57	17.30	17.20	16.69	15.19	16.33
FeO	2.35	1.37	7.95	7.29	8.34	8.09	7.51	3.37	6.50	6.32	6.14	4.84	5.15
TFe_2O_3	2.61	1.52	8.83	8.10	9.27	8.99	8.35	3.74	7.22	7.02	6.82	5.38	5.73
CaO	1.28	1.29	9.17	9.30	6.74	5.01	5.74	1.72	2.53	2.57	2.33	3.62	2.42
MgO	0.25	0.25	5.25	5.13	4.38	3.56	3.22	1.48	2.15	2.11	2.29	1.68	1.77
K_2O	1.61	1.93	0.23	0.20	1.32	1.20	1.37	2.28	3.10	2.97	3.00	2.14	2.90
Na_2O	5.01	4.59	2.14	2.44	3.43	5.37	4.70	1.93	3.36	3.53	3.44	4.26	3.70
MnO	0.04	0.07	0.12	0.12	0.25	0.22	0.20	0.05	0.06	0.06	0.06	0.08	0.06
TiO_2	0.19	0.12	0.74	0.64	1.02	1.14	1.06	0.53	0.86	0.84	0.81	0.71	0.75
P_2O_5	0.01	0.00	0.13	0.10	0.21	0.33	0.32	0.08	0.27	0.27	0.27	0.22	0.24
LOI	1.74	1.81	3.27	3.90	2.69	2.24	2.00	1.00	1.16	1.12	1.21	1.67	1.05
Total	99.90	99.90	99.86	99.88	99.86	99.85	99.86	99.86	99.82	99.83	99.84	99.88	99.85
Trace and REE elements (ppm)													
Li	2.46	3.68	24.30	23.30	10.90	10.50	10.80	33.90	38.00	36.80	30.00	29.90	32.60
Be	2.05	1.42	0.44	0.39	1.04	0.97	0.99	1.48	1.95	1.99	2.06	1.80	1.93
Sc	8.15	5.30	26.30	24.20	27.90	22.50	22.10	8.44	16.90	16.10	15.50	11.60	12.00
V	22.60	4.13	201.00	172.00	170.00	146.00	135.00	93.50	87.20	87.30	88.20	69.00	74.50
Cr	10.10	6.30	25.00	27.00	25.10	12.60	13.10	47.20	44.90	46.00	41.40	39.20	39.60
Co	1.09	0.56	31.00	30.00	22.50	16.30	15.80	8.74	17.40	16.50	15.60	10.70	11.70
Ni	2.22	2.05	27.50	26.50	18.50	6.51	6.58	15.40	23.80	22.30	21.50	15.10	15.80
Cu	5.00	2.00	47.20	43.10	11.20	10.90	14.80	9.97	11.20	15.30	13.10	22.90	15.40
Zn	24.60	17.40	66.40	59.00	121.00	129.00	110.00	43.20	101.00	94.60	91.90	73.80	78.70
Ga	20.20	16.40	17.70	17.80	19.00	20.70	20.80	13.70	22.30	22.40	21.90	18.50	19.80
Rb	43.70	45.30	6.09	4.98	28.10	25.80	30.20	150.00	107.00	104.00	105.00	74.90	92.00
Sr	73.30	89.90	746.00	672.00	631.00	521.00	652.00	493.00	739.00	702.00	760.00	263.00	239.00
Y	42.00	31.80	14.90	12.90	34.40	33.80	35.10	17.10	28.70	27.90	28.20	25.10	25.30
Zr	334.00	234.00	52.50	47.50	82.30	88.80	110.00	191.00	211.00	206.00	192.00	217.00	223.00
Nb	16.80	12.20	1.82	1.81	4.46	4.64	4.93	9.31	13.40	13.30	12.80	11.60	12.40
Sn	3.32	2.30	0.42	0.39	0.81	1.04	1.73	1.19	1.93	1.68	1.84	1.51	1.59
Cs	0.14	0.24	0.63	0.59	0.90	0.85	1.11	14.10	10.90	11.60	5.12	3.96	4.59
Ba	531.00	644.00	227.00	207.00	347.00	328.00	386.00	495.00	759.00	694.00	653.00	510.00	736.00
La	44.80	34.10	7.58	6.62	15.10	18.80	18.70	29.80	42.50	41.60	43.00	36.30	37.10
Ce	88.60	68.00	16.00	14.40	34.90	42.90	43.00	62.00	90.90	87.90	91.10	74.50	77.60
Pr	9.80	7.56	2.05	1.86	4.87	5.88	5.76	6.72	9.95	9.63	9.80	8.23	8.58
Nd	37.50	29.20	9.09	8.18	22.70	26.90	27.10	25.10	37.70	36.60	37.00	31.20	32.50
Sm	7.53	5.57	2.36	1.92	6.00	6.68	6.28	4.69	7.21	6.97	7.10	5.93	6.03
Eu	1.19	0.71	0.85	0.76	2.03	2.38	2.26	0.98	1.59	1.57	1.51	1.34	1.41
Gd	6.52	5.05	2.50	2.29	6.29	6.61	6.84	3.89	6.37	6.17	6.10	5.13	5.13
Tb	1.07	0.84	0.41	0.37	0.97	0.98	1.01	0.53	0.89	0.86	0.89	0.74	0.76
Dy	6.87	5.01	2.47	2.28	5.88	5.98	6.21	3.05	5.27	4.85	4.89	4.31	4.30
Ho	1.47	1.07	0.55	0.49	1.29	1.22	1.27	0.60	0.98	1.00	0.97	0.89	0.85
Er	4.47	3.15	1.51	1.32	3.63	3.45	3.66	1.77	2.90	2.68	2.88	2.48	2.58
Tm	0.69	0.49	0.23	0.20	0.56	0.51	0.52	0.26	0.43	0.44	0.43	0.40	0.39
Yb	4.55	3.11	1.36	1.26	3.37	3.12	3.09	1.59	2.47	2.47	2.49	2.10	2.21
Lu	0.73	0.51	0.23	0.19	0.52	0.50	0.52	0.26	0.42	0.41	0.39	0.36	0.36
Hf	8.22	6.49	1.53	1.38	2.39	2.73	3.13	5.07	5.52	5.26	5.08	5.67	5.81
Ta	0.96	0.73	0.11	0.09	0.22	0.25	0.26	0.58	0.78	0.76	0.76	0.68	0.74
Tl	0.18	0.15	0.04	0.03	0.16	0.15	0.17	0.61	0.67	0.65	0.63	0.54	0.64
Pb	8.59	8.48	3.78	3.23	13.30	10.90	13.80	17.80	21.20	21.60	19.00	16.20	15.50
Th	10.70	7.47	0.81	0.83	1.33	1.71	1.76	8.18	9.03	8.81	9.31	8.30	9.04
U	2.37	1.13	0.17	0.17	0.34	0.40	0.43	2.59	1.61	1.46	1.53	1.98	2.28
K_2O+Na_2O	6.62	6.52	2.36	2.64	4.75	6.56	6.07	4.21	6.46	6.50	6.44	6.40	6.60
A/CNK	1.14	1.12	0.95	0.92	0.85	0.87	0.87	1.21	1.28	1.26	1.27	0.95	1.20
A/NK	1.41	1.40	5.14	4.61	2.32	1.65	1.85	1.87	1.95	1.91	1.87	1.63	1.77
$Mg^{\#}$	14.34	22.39	51.46	53.04	45.72	41.41	40.77	41.37	34.69	34.86	37.45	35.70	35.51
Eu/*Eu	0.51	0.40	1.06	1.11	1.00	1.08	1.05	0.68	0.70	0.72	0.69	0.73	0.76
$(La/Yb)_N$	6.64	7.39	3.76	3.54	3.02	4.06	4.08	12.64	11.60	11.35	11.64	11.65	11.32
$(Nb/La)_N$	0.36	0.34	0.23	0.26	0.28	0.24	0.25	0.30	0.30	0.31	0.29	0.31	0.32

390 Ma, including granite with age of 384.7±2.5 Ma (Wang et al., 2014) and volcanic rocks with 378.3±2.6 Ma and 383.2±3.4 Ma reported from the Badangshan Formation in this paper. The volcanic rocks of Badangshan Formation are generally characterized by enrichment of LREE and LILE and depletion of HFSE. On the Sr/Y versus Y diagrams (Fig. 11d),the samples of the rhyolite and basaltic andesite were plotted in the field of typical arc rocks, on the Nb*2-Zr/4-SiO_2 and Hf/3-Th-Ta diagrams (Fig. 11e and f), basalt were plotted in the

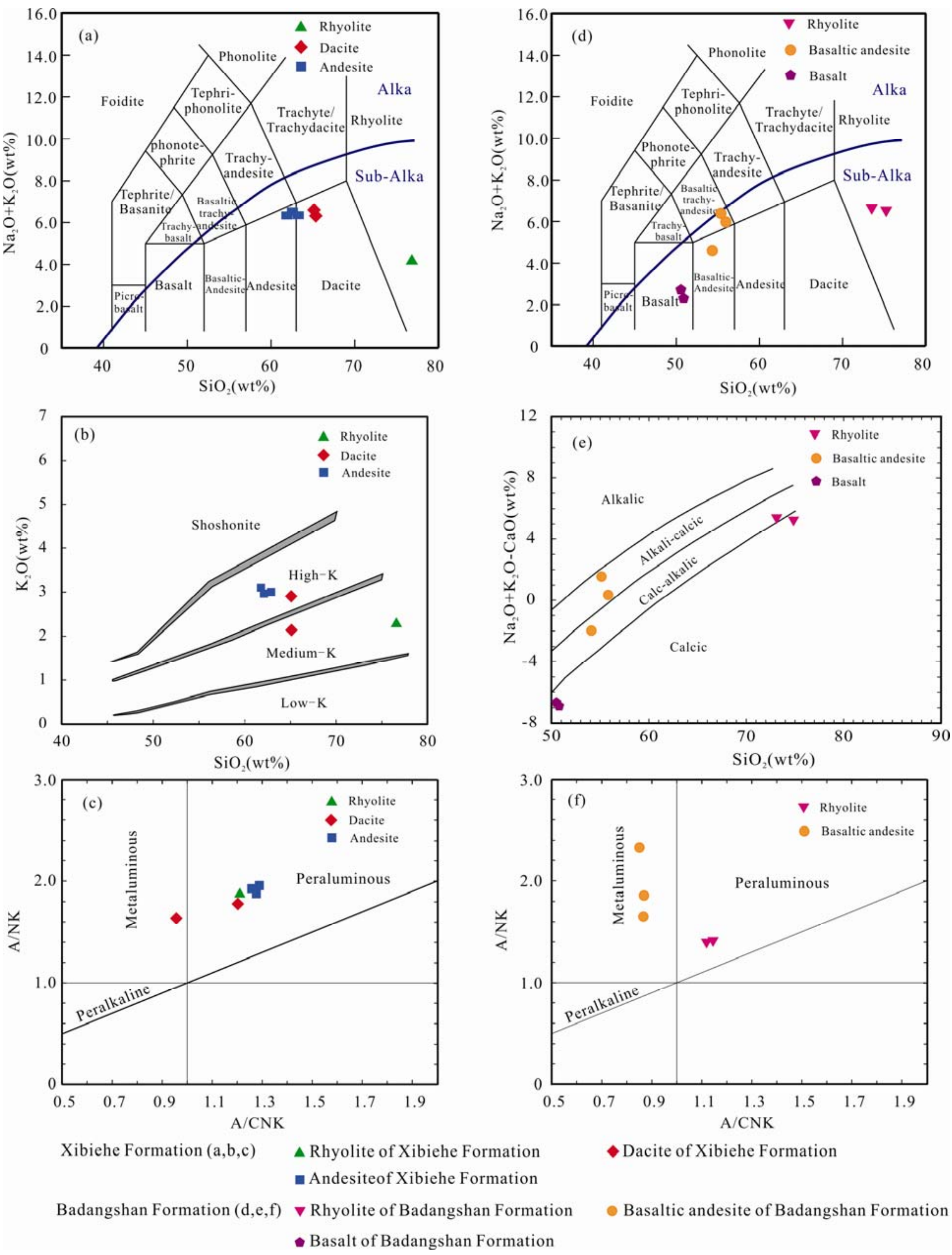

Fig. 9. Classification diagrams for the Early–Middle Paleozoic igneous rocks from Chifeng area.
(a, d) Total alkali versus SiO_2 (TAS) diagrams with fields from Irvine and Baragar (1971); (b) SiO_2 versus K_2O diagrams with fields from Peccerillo and Taylor (1976); (c, f) A/CNK versus A/NK diagram with fields from Maniar and Piccoli (1989); (e) (Na_2O+K_2O-CaO) versus SiO_2 diagram with fields from Frost et al., (2001).

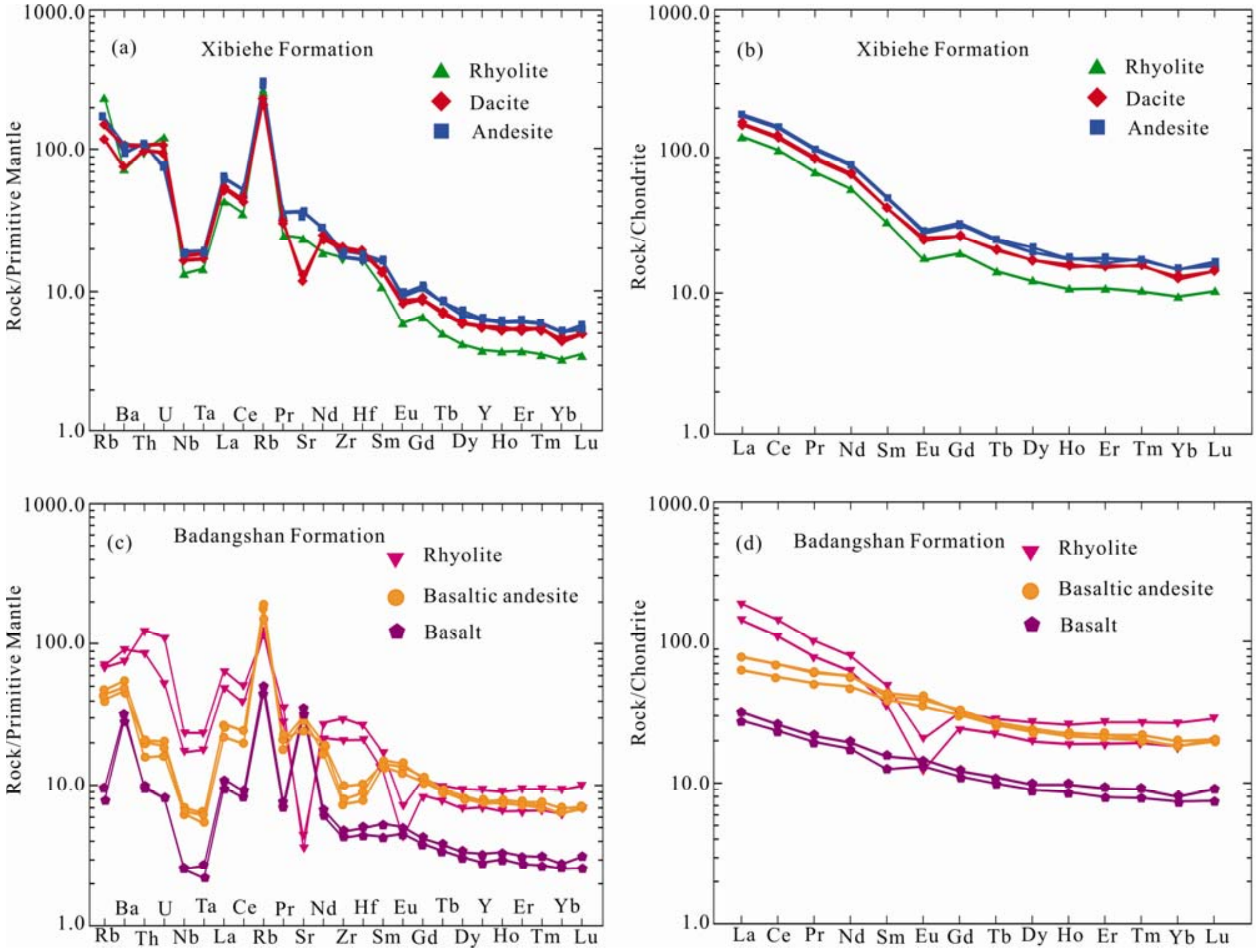

Fig. 10. Chondrite-normalized REE patterns (a, c) and primitive-mantle-normalized trace element spidergrams (b, d) for the Early–Middle Paleozoic igneous rocks of Chifeng area. Chondrite and primitive-mantle values are from Boynton (1984) and Sun and McDonough (1989), respectively.

field of volcanic-arc basalt, suggesting that volcanic rocks of the Badangshan Formation were developed in an continental arc setting. Moreover, basaltic andesite and basalt display positive Sr anomalies, and basalts have very low Nb/La values («1), shows that fluid is involved in magma evolution and basalt is contaminated by continental crust.

5.3 Tectonic significance of the accretionary prism in Qiganmiao area

According to discussion about paleogeographic frame, the southward subduction of the PAO under the NCC resulted in an accretionary prism represented by the mélange in Qiganmiao area, where zircon U-Pb ages of 446.0±6.3 Ma and 1104±27 Ma have been acquired and been interpreted as the metamorphic and forming ages for the gabbro and two-mica quartz schist, respectively. It seems that the gabbro represents the early Paleozoic ocean crust of the PAO, and the two-mica quartz schist, slice of the SHB (Fig. 1, Xu et al., 2013). Therefore, the early Paleozoic accretionary prism with different kind of blocks formed during the southward subduction of the PAO and represents the suture between the NCC and CAOB.

Previous research results indicate that high-pressure metamorphic events characterized by blueschist and phengite were developed in the Ondoe Sum area of the middle segment of the SOB, with the metamorphic ages of 445.6±1.5 Ma, 453.2±1.8 Ma and 449.4±1.8 Ma (Fig. 1, Tang et al., 1992; De Jong et al., 2006). Another age of this strong metamorphic belt found in Tugurige area, 150km west of Ondor Sum, is 440.3±7.2 Ma（Liao, et al., 2015）, indicating that both regions were affected by the same early-middle orogeny. In this study, the metamorphic age of the gabbro was determined to be 446.0±6.3 Ma in the accretionary prism of the eastern segment of the SOB, which was consistent with ages of the western metamorphic event, providing evidence for the eastward extension of the SOB. All metamorphic ages in the SOB that represent the early-middle Paleozoic border between the NCC and CAOB provide new constraint for the closure time of the PAO.

5.4 The early-middle Paleozoic tectonic evolution

According to our field investigation, geochronological and geochemical data, combined with previous research in this area, a tectonic evolutionary model can be suggested

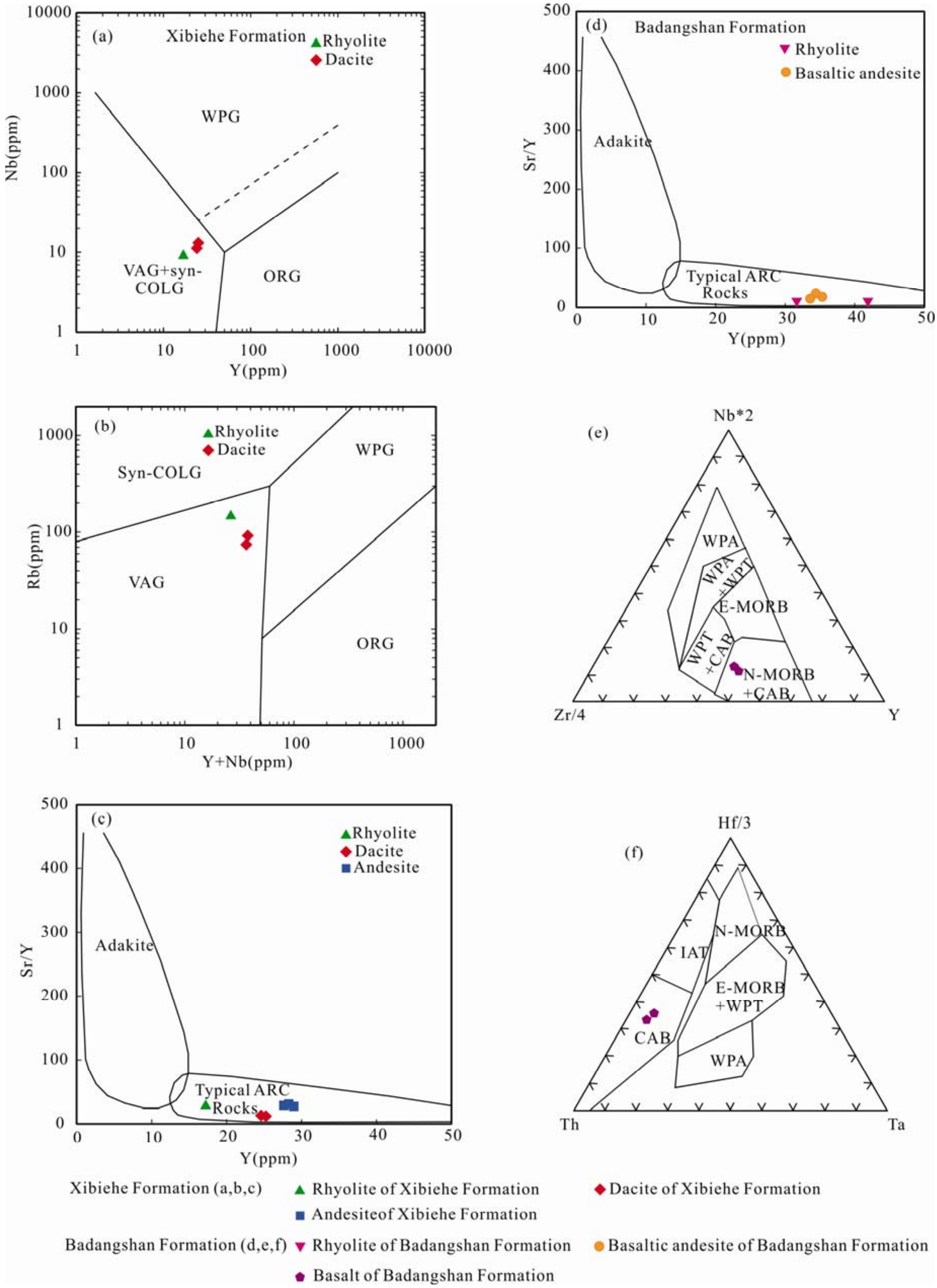

Fig. 11. Discrimination diagrams for Early–Middle Paleozoic igneous rocks of Chifeng area.

(a) Nb versus Y diagrams with fields from Pearce (1984); (b) Rb versus Y and Nb diagrams with fields from Pearce (1984); (c, d) Sr/Y versus Y diagram with fields from Defant and Drummond (1990); (e) Nb*2-Zr/4-SiO_2 diagram with fields from Meschede (1986); (f) Hf/3-Th-Ta diagram with fields from Wood (1980); IAT: Island Arc Tholeiites; CAB: Calc Alkaline Basalts; N-MORB: N-type Mid-Ocean Ridge Basalts; E-MORB: E-type Mid-Ocean Ridge Basalts; WPT: Within-plate Tholeiites; WPA: Within-plate Alkaline Basalts.

as following (Fig. 12):

(a) Before 446Ma: there were the SHB in the north, the NCC in the south and the PAO between them, respectively. No subduction of the PAO occurred between the SHB and NCC (Fig. 12a);

(b) From 446 Ma to 380 Ma: there was a southward subduction of the PAO beneath the northern continental margin of the NCC, forming the Qiganmiao accretionary prism and the first stage magmatism of the continental arc belt in Jiefangyingzi–Wutonghua area;

(c) From 380 Ma to 360 Ma: the southward subduction of the PAO terminated, which followed by a continent-continent collision that resulted in the formation of a molasse basin in Sidaozhangpeng area between the Jiefangyingzi continent arc belt and the NCC. The basin filled by the Sidaozhangpeng Formation characterized by a set of cyclic conglomerates, sandstone and fine sandstone assemblages.

At 360 Ma, a set of bimodal volcanic rocks developed in Chaotugou area, Aohan Banner to the south of our study area (Sun et al., 2017), indicating that the northern margin of the North China Croton began to enter a post-orogenic extensional stage at the end of the Late Devonian.

6 Conclusions

(1) Three tectonic units have been recognized in the Chifeng area, Inner Mongolia, from north to south, including the Qiganmiao accretionary prism, Jiefangyingzi arc belt and Sidaozhangpeng molasse basin, which composed an Andean-type active continent margin during the early to middle Paleozoic.

(2) The Qiganmiao accretionary prism is characterized by a mélange that consists of gabbro, two-mica quartz schist and basic volcanic rock blocks and heterogeneously deformed marble matrix. The prism formed during the early to middle Paleozoic southward subduction of the PAO and represents the suture between the NCC and CAOB.

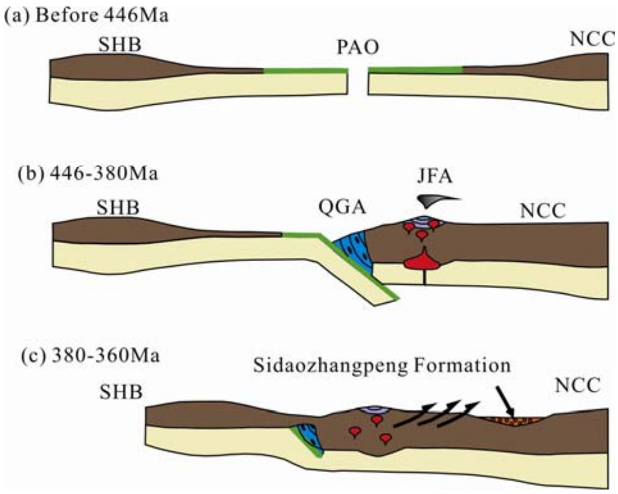

Fig. 12. Schematic cartoons illustrating the tectonic evolution of Chifeng trench-arc-basin system (after Xu et al., 2013).
SHB: SongLiao-Hunshandake Bolck; NCC: North China Croton; PAO: Paleo Asian Ocean; QGA: Qiganmiao accretionary prism; JFA: Jiefangyingzi arc belt.

(3) Tectonic evolution of the CAOB in Chifeng area can be divided into three stages, including a development of the subduction-free PAO before 446 Ma, a subduction of the PAO and arc-related magmatism during 446-380 Ma, and formation of a molasse basin during 380–360 Ma.

Acknowledgements

We thank Zhang Liyang and Wang Zhiwei for their support in the field, Ma Fang for her help in ICP-MS analyses of zircons, and Yang Bin for his help in chemical analyses. We gratefully acknowledge constructive reviews from two anonymous reviewers. This study was supported by grants from National Key R&D Program of China (2017YFC0601302), the NSF of China (41672214) and Geological Survey Project of China Geological Survey (DD20189612, DD20190004).

Manuscript received Feb. 25, 2019
accepted Dec. 20, 2019
associate EIC YANG Jingsui
edited by LIU Lian

References

Andersen, T., 2002. Correction of common lead in U-Pb analyses that do not report ^{204}Pb. Chemical Geology, 192(1-2): 59–79.

Badarch, G., Cunningham, W.D., and Windley, B.F., 2002. A new terrane subdivision for Mongolia: implications for the Phanerozoic crustal growth of Central Asia. Journal of Asian Earth Sciences, 21(1): 87–110.

Boynton, W.V., 1984. Geochemistry of the rare earth elements: Meteorite studies. In: Henderson, P. (Ed.), Rare Earth Element Geochemistry. Elsevier, Amsterdam, 63–114.

Chen, B., Jahn, B.M., and Tian, W., 2009. Evolution of the Solonker suture zone: Constraints from zircon U-Pb ages, Hf isotopic ratios and whole-rock Nd-Sr isotope compositions of subduction- and collision- related magmas and forearc sediments. Journal of Asian Earth Sciences, 34(3): 245–257.

Chen, B., Jahn, B., Wilde, S., Bei, X., Jahn, B., Griffin, W.L., Windley, B.F., 2000. Two contrasting Paleozoic magmatic belts in northern Inner Mongolia, China; petrogenesis and tectonic implications. Tectonophysics, 328(1-2): 157–182.

Chen, J.S., Liu, M., Li, B., Li,W., Li, W.W., Yang, F., and Wang, Y., 2017. Zircon U-Pb chronology and geochemical characteristics of Late Silurian monzogranite in Ongniud Bannar, Inner Mongolia. Geological Bulletin of China, 36(8): 1359–1368 (in Chinese with English abstract).

Demoux, A., Kröner, A., Badarch, G., Jian, P., Tomurhuu, D., and Wingate, M.T.D., 2009. Zircon Ages from the Baydrag Block and the Bayankhongor Ophiolite Zone: Time Constraints on Late Neoproterozoic to Cambrian Subduction- and Accretion- Related Magmatism in Central Mongolia. Journal of Geology, 117(4): 377–397.

Defant, M.J., and Drummond, M.S., 1990. Derivation of some modern arc magmas by melting of young subducted lithosphere. Nature, 347(6294): 662–665.

De Jong, K., Xiao, W.J., Windley, B.F., Masago, H., and Lo, C.H., 2006. Ordovician ^{40}Ar/^{39}Ar phengite ages from the blueschist-facies Ondor Sum subduction-accretion complex (Inner Mongolia) and implications for the Early Paleozoic history of continental blocks in China and adjacent areas. American Journal of Science, 306(10): 799–845.

Deng, Z.B., Liu, S.W., Zhang, L.F.,Wang, Z.Q., Wang,W., Yang, P.T., Luo, P., and Guo, B.R., 2014. Geochemistry, zircon U-Pb and Lu-Hf isotopes of an Early Cretaceous intrusive suite in northeastern Jiangxi Provenance, South China block: implications for petrogenesis, crust/mantle interactions and geodynamic processes. Lithos, 200–201(1): 334–354.

Frost, B.R., Barnes, C.G., Collins, W.J., Arculus, R.J., Ellis, D.J., and Frost, C.D., 2001. A geochemical classification for granitic rocks. Journal of Petrology, 42(11): 2033–2048.

Han, B.F., He, G.Q., Wang, X.C., and Guo, Z.J., 2011. Late Carboniferous collision between the Tarim and Kazakhstan-Yili terranes in the western segment of the South Tian Shan Orogen, Central Asia, and implications for the Northern Xinjiang, western China. Earth-Science Reviews, 109(3-4): 74–93.

Han, B.F., Wang, S.G., Jahn, B.M., Hong, D.W., Hiroo, K., and Sun, Y.L., 1997. Depleted-mantle source for the Ulungur River A-type granites from North Xinjiang, China: geochemistry and Nd-Sr isotopic evidence, and implications for Phanerozoic crustal growth. Chemical Geology, 138(3-4): 135–159.

He, Y., Xu, B., Zhang, L.Y., and Zhang, Y.J., 2018. Discovery of a Late Devonian retroarc foreland basin in Sunid Zuoqi, Inner Mongolia and its tectonic implications. Acta Petrologica Sinica, 34(10): 3071–3082 (in Chinese with English abstract).

Hu, X., Xu, C., and Niu, S., 1990. Evolution of the Early Paleozoic Continental Margin in Northern Margin of the North China Platform. Beijing: Peking University Press, 215 (in Chinese with English abstract).

Hong, D.W., Wang, S.G., Xie, X.L., Zhang, J., and W,T., 2003. Correlation between Continental Crustal Growth and the Supercontinental Cycle: Evidence from the Granites with Positive ε_{Nd} in the Central Asian Orogenic Belt. Acta Geologica Sinica, 77(2): 203–209.

Hong, D., Wang, S., Han, B., and Jin, M., 1996. Post-orogenic alkaline granites from China and comparisons with anorogenic alkaline granites elsewhere. Journal of Asian Earth Sciences, 13(1): 13–27.

Hsü, K.J., Wang, Q., Li, L., Hao, J., 1991. Geologic evolution of the Neimonides: a working hypothesis. Eclogae Geol Helv. Eclogae Geologicae Helvetiae, 84(1): 1–31.

IMBGMR (Inner Mongolian Bureau of Geology and Mineral Resources), 1991. Regional Geology of Inner Mongolian Autonomous Region. Beijing: Geological Publishing House, 726 (in Chinese with English abstract).

Irvine, T.H., and Baragar, W.R.A., 1971. A guide to the chemical classification of the common volcanic rocks. Canadian Journal of Earth Sciences, 8(5): 523–548.

Jahn, B.M., Litvinovsky, B.A., Zanvilevich, A.N., and Reichow, M., 2009. Peralkaline granitoid magmatism in the Mongolian-Transbaikalian Belt: Evolution, petrogenesis and tectonic significance. Lithos, 113(3–4): 521–539.

Jahn, B.M., Wu, F.Y., Chen, B., 2000a. Granitoids of the Central Asian Orogenic Belt and continental growth in the Phanerozoic. Transactions of the Royal Society of Edinburgh: Earth Sciences, 91: 181–193.

Jahn, B.M., Wu, F.Y., Chen, B., 2000b. Massive granitoid generation in Central Asia: Nd isotope evidence and implication for continental growth in the Phanerozoic. Episodes, 23(2): 82–92.

Jian, P., Liu, D., Kröner, A., Windley, B.F., Shi, Y., Zhanf, F., Shi, G., Miao, L., Zhang, W., Zhang, Q., Zhang, L., and Ren, J., 2008. Time scale of an early to mid-Paleozoic orogenic cycle of the long-lived Central Asian Orogenic Belt, Inner Mongolia of China: implications for continental growth. Lithos, 101(3–4): 233–259.

Khain, E.V., Bibikova, E.V., Salnikova, E.B., Kröner, A., Gibsher, A.S., Didenko, A.N., Degtyarev, K.E., and Fedotova, A.A., 2003. The Palaeo-Asian ocean in the Neoproterozoic and early Palaeozoic: new geochronologic data and palaeotectonic reconstructions. Precambrian Research, 122(1): 329–358.

Khain, E.V., Bibikova, E.V., Kröner, A., Zhuravlev, D.Z., Sklyarov, E.V., Fedotova, A.A., and Kravchenko-Berezhnoy, I.R., 2002. The most ancient ophiolite of the Central Asian fold belt: U-Pb and Pb-Pb zircon ages for the Dunzhugur Complex, Eastern Sayan, Siberia, and geodynamic implications. Earth & Planetary Science Letters, 199(3–4): 311–325.

Kröner, A., 2010a. Zircon ages for a felsic volcanic rock and arc-related early Palaeozoic sediments on the margin of the Baydrag microcontinent, central Asian orogenic belt, Mongolia. Journal of Asian Earth Sciences, 42(5): 1008–1017.

Kröner, A., Lehmann, J., Schulmann, K., Demoux, A., Lexa, O., Tomurhuu, D., Štípská, P., Liu, D., and Wingate, M.T.D., 2010b. Lithostratigraphic and geochronological constraints on the evolution of the Central Asian Orogenic Belt in SW Mongolia: Early Paleozoic rifting followed by late Paleozoic accretion. American Journal of Science, 310(7): 523–574.

Kröner, A., Windley, B.F., Badarch, G., Tomurtogoo, O., Hegner, E., Jahn, B.M., Gruschka, S., Khain, E.V., Demoux, A., and Wingate, M.T.D., 2007. Accretionary growth and crust-formation in the Central Asian Orogenic Belt and comparison with the Arbian-Nubian shield. Memoir of the Geological Society of America, 200: 181–209.

Li, J.Y., Zhang, J., Yang, T.N., L,Y.P., Sun, G.H., Zhu, Z.X., and Wang, L.J., 2009. Crustal Tectonic Division and Evolution of the Southern Part of the North Asian Orogenic Region and Its Adjacent Areas. Journal of Jilin University (Earth Science Edition), 39(4): 584–605.

Li, J.Y., 2006. Permian geodynamic setting of Northeast China and adjacent regions: closure of the Paleo-Asian Ocean and subduction of the Paleo-Pacific Plate. Journal of Asian Earth Sciences, 26(3-4): 207–224.

Li, R.B., Xu, B., Zhao, P., Tong, Q.L., and Zhang, J.R., 2014. The discovery of blueschistfacies rock in Airgin Sum area, Erenhot, Inner Mongolia and its tectonic significance. Chinese Science Bulletin, 59(1): 66–71 (in Chinese).

Liao,W., Xu, B., Bao, Q.Z., and Zhou, Y.H., 2015. Deformation features and muscovite Ar-Ar age of the late Early Paleozoic deformed zone in the southwestern Xing'an-Mongolia Orogenic Belt. Acta Petrologica Sinica, 31(1): 80–88 (in Chinese with English abstract).

Liu, J.F., Li, J.Y., Chi, X.G., Feng, Q.W., Hu, Z.C., and Zhou, K., 2013. Early Devonian felsic volcanic rocks related to the arc-continent collision on the northern margin of North China craton-evidences of zircon U-Pb dating and geochemical characteristics. Geological Bulletin of China, 32(2–3): 267–278 (in Chinese with English abstract).

Ludwig, K.R., 2003. Isoplot /Ex, A Geochronological toolkit for Microsoft Excel version 3. 00. Berkeley: Berkeley Geochronology Center, 4: 1–70.

Maniar, P.D., and Piccoli, P.M., 1989. Tectonic discrimination of granitoids. Geological Society of America Bulletin, 101(5): 635–643.

Meschede, M., 1986. A method of discriminating between different types of mid-ocean ridge basalts and continental tholeiites with the Nb-Zr-Y diagram. Chemical Geology, 56(3–4): 207–218.

Mossakovsky, A.A., Ruzhentsev, S.V., Samygin, S.G., and Kheraskova, T.N., 1993. Central Asian fold belt; geodynamic evolution and formation history. Geotectonics, 26: 455–473.

Pearce, J.A., 1996. Sources and settings of granitic rocks. Episodes, 19(4): 120–125.

Pearce, J.A., Harris, N., and Tindle, A.G., 1984. Trace element discrimination diagrams for the tectonic interpretation of granitic rocks. Journal of Petrology, 25(4): 956–983.

Peccerillo, A., and Taylor, S.R., 1976. Geochemistry of Eocene calc-alkaline volcanic rocks from the Kastamonu area, Northern Turkey. Contributions to Mineralogy and Petrology, 58(1): 63–81.

Sengör, A.M.C., and Natal'in, B.A., 1996. Paleotectonics of Asia: fragments of a synthesis, in: Rubey Colloquium, C.U.P., Cambridge (Ed.), The Tectonic Evolution of Asia, 486–640.

Şengör, A.M.C., Natal'in, B.A., and Burtman, V.S., 1993. Evolution of the Altaid tectonic collage and Palaeozoic crustal growth in Eurasia. Nature, 364(6435): 299–307.

Shao, J.A., 1991. Crust Evolution in theMiddle Part of the NorthernMargin of Sino-Korean Plate. Beijing: Peking University Press, 136 (in Chinese with English abstract).

Shao, J.A., 1986. Early Paleozoic ophiolite in middle Inner Mongolia and its implications for reconstruct crust evolution. In: Collection of Papers on Tectonics of North China Plate. Beijing: Earthquake Publishing House, 87–101 (in Chinese).

Shi, G., Faure, M., Xu, B., Zhao, P., and Chen, Y., 2013. Structural and kinematic analysis of the Early Paleozoic

Ondor Sum-Hongqi mélange belt, eastern part of the Altaids (CAOB) in Inner Mongolia, China. Journal of Asian Earth Sciences, 66(complete): 123–139.
Sláma, J., Kosler, J., Condon, D.J., Crowley, J.L., Gerdes, A., Hanchar, J.M., Horstwood, M.S.A., Morris, G.A., Nasdala, L., Norberg, N., Schaltegger, U., Schoene, B., Tubrettk, M.N., and Whitehouse, M.J., 2008. Plešovice zircon: A new natural reference material for U-Pb and Hf isotopic microanalysis. Chemical Geology, 249(1-2): 1–35.
Sun, S.S., and McDonough, W.F., 1989. Chemical and isotopic systematics of oceanic basalts: implications for mantle composition and processes. In: Saunders, A.D., Norry, M.J. (Eds.), Magmatism in Ocean Basins, pp. 313–345.
Tang, K.D., 1992. Tectonic evolution and minerogenetic regularities of the fold belt along the Northern Margins of Sino-Korean Plate. Beijing: Peking University Press, 277 (in Chinese with English abstract).
Tang, K.D., and Zhang, Y.P. 1991. Tectonic evolution of Inner Mongolia. In: Tectonic Evolution of the Southern Margin of the Paleo-asian Composite Megasuture, Xiao, X.C., and Tang, Y.Q. (eds). Beijing: Scientific and Tectonical Publishing House, 30–53 (in Chinese with English abstract).
Wang, X.A., Li, S.C., Xu, Z.Y., and Zhu, K., 2016. Neoarchaean quartz diorites in the Jiefangyingzi area, Central Asian Orogenic Belt: geological and tectonic significance. International Geology Review, 58(3): 358–370.
Wang, X.A., 2014. Tectonic evolution in the central segment of the northern margin of the north china plate from early Paleozoic to devonian. Changchun:Jilin University (Ph. D thesis), 1–109 (in Chinese).
Wood, D.A., 1980. The application of a Th-Hf-Ta diagram to problems of tectonomagmatic classification and to establishing the nature of crustal contamination of basaltic lavas of the British Tertiary volcanic province. Earth and Planetary Science Letters, 50(1): 11–30.
Wu, Y.B., Zheng, Y.F., 2004. Genesis of zircon and its constraints on interpretation of U-Pb age. Chinese Science Bulletin, 49(16): 1554–1569 (in Chinese).
Xia, B.D., Fang, Z., Lv, H.B., and Yu, J.H.,1989.Molasse and global tectonics. Experimental Petroleum Geology, 11(4): 314–319 (in Chinese with English abstract).
Xiao, W.J., Windley, B.F., Huang, B.C., Han, C.M., Yuan, C., Chen, H.L., Sun, M., Sun, S., and Li, J.L., 2009. End-Permian to mid-Triassic termination of the accretionary processes of the southern Altaids: implications for the geodynamic evolution, Phanerozoic continental growth, and metallogeny of Central Asia. International Journal of Earth Sciences, 98(6): 1189–1217.
Xiao, W.J., Windley, B.F., Badarch, G., Sun, S., Li, J., Qin, K., and Wang, Z., 2004. Palaeozoic accretionary and convergent tectonics of the southern Altaids: implications for the growth of Central Asia. Journal of the Geological Society, 161: 339–342.
Xiao, W.J., Windley, B., Hao, J., and Zhai, M.G., 2003. Accretion leading to collision and the Permian Solonker suture, Inner Mongolia, China: termination of the Central Asian Orogenic Belt. Tectonics, 22(6): 1069–1089.
Xu, B., Charvet, J., Chen, Y., Zhao, P., and Shi, G.Z., 2013. Middle Paleozoic convergent orogenic belts in western Inner Mongolia (China): framework, kinematics, geochronology and implications for tectonic evolution of the Central Asian Orogenic Belt. Gondwana Research, 23(4): 1342–1364.
Xu, B., Liu, S.W., Wang C.Q., and Zheng, H.F., 2001. Geologic map (1:50,000) and geologic report of Tugurige area, Inner Mongolia, Peking University.
Xu, B., and Chen, B., 1997. Framework and evolution of the middle Paleozoic orogenic belt between Siberian and North China Plates in northern Inner Mongolia. Science in China (series D), 40(5): 463–469.
Xu, B., and Chen, B., 1993. The opposite subduction and collision between the Siberian and Sino-Korean plates during the early-middle Paleozoic. Report No: 4 of the IGCP Projrct 283: Geodynamic Evolution of Paleoasian Ocean, Novosibirsk, USSR, 148–150.
Yarmolyuk V.V., KovalenkoV.I., Sal'nikova E.B., Kovach V.P., Kozlovsky A.M., Kotov A.B., and Lebedev V.I., 2008. Geochronology, Igneous Rocks and Formation of the Late Paleozoic South Mongolian Active Margin of the Siberian Continent. Stratigraphy and Geological Correlation, 16(2): 162–181.
Zhang, J.F., Liu, Z.H.,Guan,Q.B.,Xu,Z.Y.,Wang,X.A., and Zhu,K., 2017. Age and geological significance of Xuniwusu Formation from Bainaimiao area of Sonid Youqi, Inner Mongolia. Acta Petrologica Sinica, 33(10): 3147–3160 (in Chinese with English abstract).
Zhang, J.R., Wei, C.J., and Chu, H., 2018. New model for the tectonic evolution of Xing'an-Inner Mongolia Orogenic Belt:Evidence from four different phases of metamorphism in Central Inner Mongolia. Acta Petrologica Sinica, 34(10): 2857–2872 (in Chinese with English abstract).
Zhang, Y.P., Su, Y.Z., and Li, J.C., 2010. Regional tectonic significance of the Late Silurian Xibiehe Formation in central Inner Mongolia, China. Geological Bulletin of China, 29(11): 1599–1605 (in Chinese with English abstract).
Zhang, Y.P., and Tang, K.D., 1989. Pre-Jurassic tectonic evolution of intercontinental region and the suture zone between the North China and Siberian platforms. Journal of Southeast Asian Earth Sciences, 3(1-4): 47–55.

About the first author

YAN Linjie, male, born in 1991 in Shaoyang City, Hunan Province; Ph. D. candidate majoring in Continental Dynamics and Natural Resource Engineering, Peking university. He is mainly engaged in regional geotectonic work. E-mail: yanlj@pku.edu.cn.

About the corresponding author

XU Bei, male, born in 1954 in Zhangjiakou City, Hebei Province; professor of tectonics at school of Earth and Space Science, Peking university; graduated from China University of Geosciences (Beijing). He is now interested in regional geotectonic research. E-mail: bxu@pku.edu.cn.